ANALYSIS OF TRANSIENT FLOW FOR REGENERATIVE LIQUID-PROPELLANT GUN CONCEPTS

FINAL REPORT

SAIC®
Science Applications International Corporation
An Employee-Owned Company

2

ANALYSIS OF TRANSIENT FLOW FOR REGENERATIVE LIQUID-PROPELLANT GUN CONCEPTS

FINAL REPORT

September 1988

Raymond B. Edelman
Mostafa A. Rizk
M. Yousef Bahadori

Submitted to:

U.S. Army Research Office
P.O. Box 12211
Research Triangle Park, NC 27709

Contract No. DAAG29-83-C-0029

Submitted by:

Science Applications International Corporation
Combustion Science and Advance Technology Department
9760 Owensmouth Avenue
Chatsworth, CA 91311

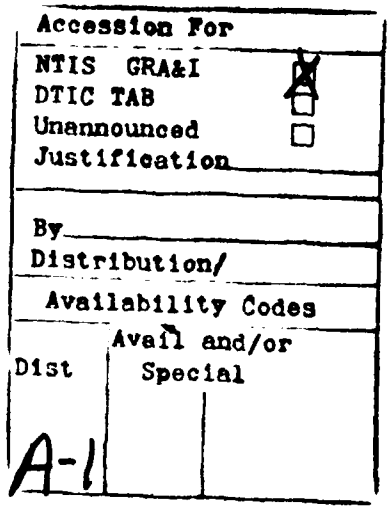

The view, opinions, and/or findings contained in this report are those of the authors and should not be construed as an official Department of the Army position, policy, or decision, unless so designated by other documentation.

UNCLASSIFIED
SECURITY CLASSIFICATION OF THIS PAGE

REPORT DOCUMENTATION PAGE

1a. REPORT SECURITY CLASSIFICATION Unclassified	1b. RESTRICTIVE MARKINGS
2a. SECURITY CLASSIFICATION AUTHORITY	3. DISTRIBUTION/AVAILABILITY OF REPORT Approved for public release; distribution unlimited.
2b. DECLASSIFICATION/DOWNGRADING SCHEDULE	
4. PERFORMING ORGANIZATION REPORT NUMBER(S)	5. MONITORING ORGANIZATION REPORT NUMBER(S) ARO 20572.1-EG
6a. NAME OF PERFORMING ORGANIZATION Science Applications International Corporation 6b. OFFICE SYMBOL (If applicable)	7a. NAME OF MONITORING ORGANIZATION U. S. Army Research Office
6c. ADDRESS (City, State, and ZIP Code) 9760 Ownesmouth Avenue Chatsworth, California 91311	7b. ADDRESS (City, State, and ZIP Code) P. O. Box 12211 Research Triangle Park, NC 27709-2211
8a. NAME OF FUNDING/SPONSORING ORGANIZATION U. S. Army Research Office 8b. OFFICE SYMBOL (If applicable)	9. PROCUREMENT INSTRUMENT IDENTIFICATION NUMBER DAAG-29-83-C-0029
8c. ADDRESS (City, State, and ZIP Code) P. O. Box 12211 Research Triangle Park, NC 27709-2211	10. SOURCE OF FUNDING NUMBERS PROGRAM ELEMENT NO. / PROJECT NO. / TASK NO. / WORK UNIT ACCESSION NO.

11. TITLE (Include Security Classification)
Analysis of Transient Flow for Regenerative Liquid-Propellant Gun Concepts

12. PERSONAL AUTHOR(S)
Raymond B. Edelman, Mostafa A. Rizk and M. Yousef Bahadori

13a. TYPE OF REPORT	13b. TIME COVERED	14. DATE OF REPORT (Year, Month, Day)	15. PAGE COUNT
Final	FROM 10/1/83 TO 10/31/87	1988/09/09	vi + 44

16. SUPPLEMENTARY NOTATION
The view, opinions and/or findings contained in this report are those of the author(s) and should not be construed as an official Department of the Army position, policy, or decision, unless so designated by other documentation.

17. COSATI CODES			18. SUBJECT TERMS (Continue on reverse if necessary and identify by block number)
FIELD	GROUP	SUB-GROUP	Liquid-propellant guns, Orifice flow, Regenerative Injection, Computational fluid dynamics, Transient flow, Two-dimensional modeling.

19. ABSTRACT (Continue on reverse if necessary and identify by block number)
This research activity has involved the development of a two-dimensional, transient simulation of the interior ballistics process in regenerative liquid-propellant guns, with emphasis on the description of the flow inside the injector covering the domain of the flow path from the propellant chamber to the exit of the annular orifice injector. This report presents the prediction of the onset and temporal growth of recirculation zones inside an orifice with fixed, spatially varying cross-sectional area, the direct prediction of discharge coefficients for moving-boundary orifice flows and comparisons with experimental data, and a study of grid resolution effects in a straight annular orifice for which an analytical solution for steady flow exists.

20. DISTRIBUTION/AVAILABILITY OF ABSTRACT ☒ UNCLASSIFIED/UNLIMITED ☐ SAME AS RPT. ☐ DTIC USERS	21. ABSTRACT SECURITY CLASSIFICATION Unclassified
22a. NAME OF RESPONSIBLE INDIVIDUAL	22b. TELEPHONE (Include Area Code) / 22c. OFFICE SYMBOL

DD FORM 1473, 84 MAR 83 APR edition may be used until exhausted. All other editions are obsolete.

SECURITY CLASSIFICATION OF THIS PAGE
UNCLASSIFIED

TABLE OF CONTENTS

LIST OF FIGURES

1. INTRODUCTION

Liquid-propellant guns (LPGs) represent a concept in gun design that offers many advantages over conventional solid-propellant weapons. Higher impulses at lower peak pressures, cooler operation, reduced erosion, improved propellant management, and elimination of the cartridge are the major advantages, all of which lead to a lightweight, low-volume gun system that is capable of high muzzle velocities at sustained, higher rates of fire.

The advantages of liquid propellants have led to exploratory development activities on bulk-loaded and regenerative, direct-injection gun concepts. In the former, the propellant is loaded in bulk and ignited; see Fig. 1.1(a). In the latter concept, a split chamber is used in which the propellant is sprayed through a regeneratively activated piston into the forward combustion chamber, while the force to drive the piston into the propellant section is derived from the combustion process; see Fig. 1.1(b).

Test results on both concepts have exhibited unexplained phenomena that are manifest in erratic behavior in the pressure-time traces. Bulk-loaded gun firings have exhibited unacceptable shot-to-shot variability in the pressure-time traces (Fig. 1.2). Pressure-time traces obtained from regenerative gun firings exhibit a variety of oscillations during the combustion process, an example of which is shown in Fig. 1.3.

These observations have not been explained and, although no catastrophic failures have been reported to-date, the sources of these variabilities require a more fundamental understanding of the interior ballistics process in order to ensure that the relationship between gun design and performance is predictable. Research conducted to date has begun to provide a basis for this needed understanding.

The overall objective of the present study was to develop a fundamental understanding of the interior ballistics process in liquid-propellant guns,

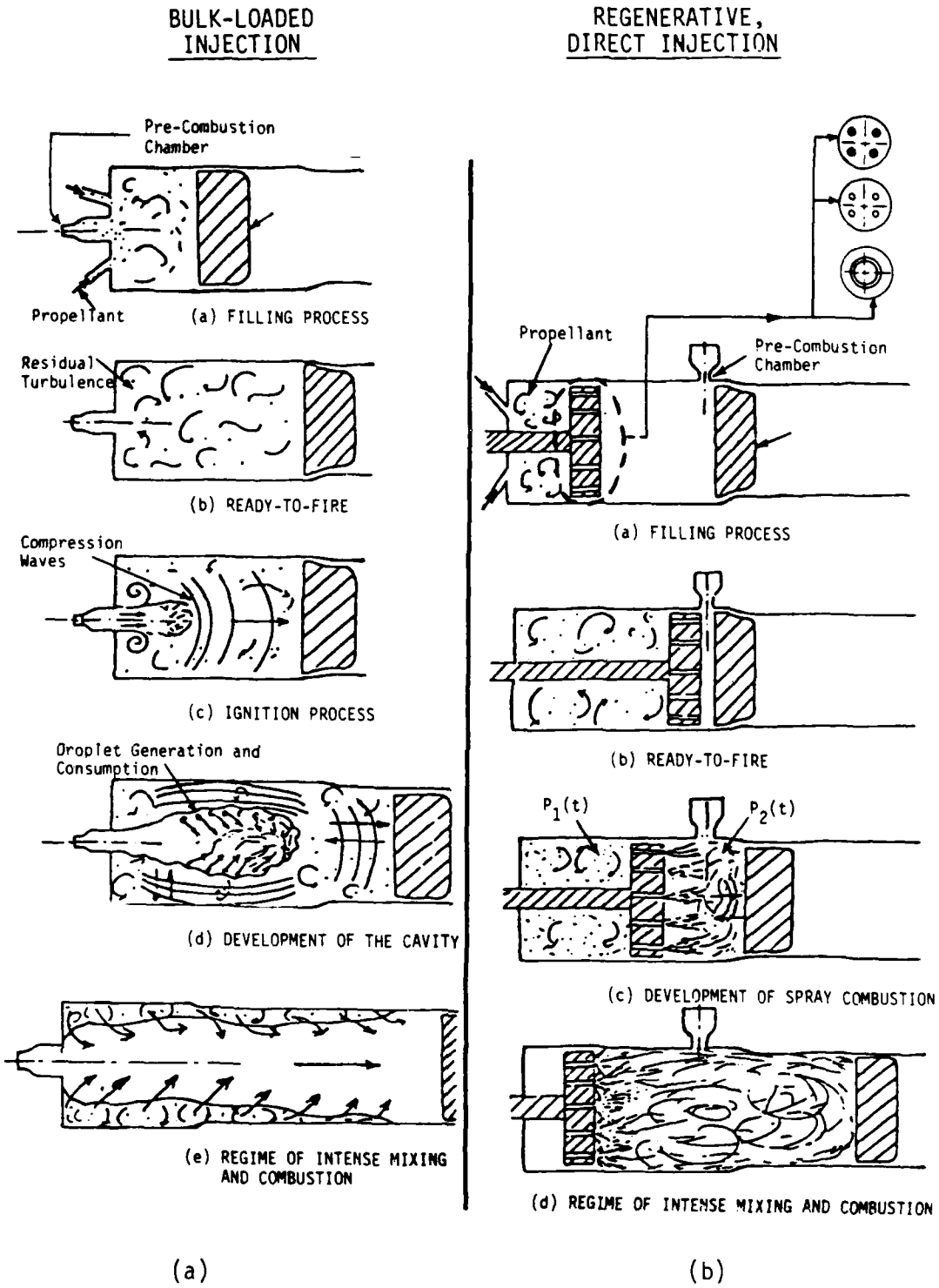

Fig. 1.1. Schematic of the LPG firing cycle for (a) bulk-loaded injection, and (b) regenerative, direct injection.

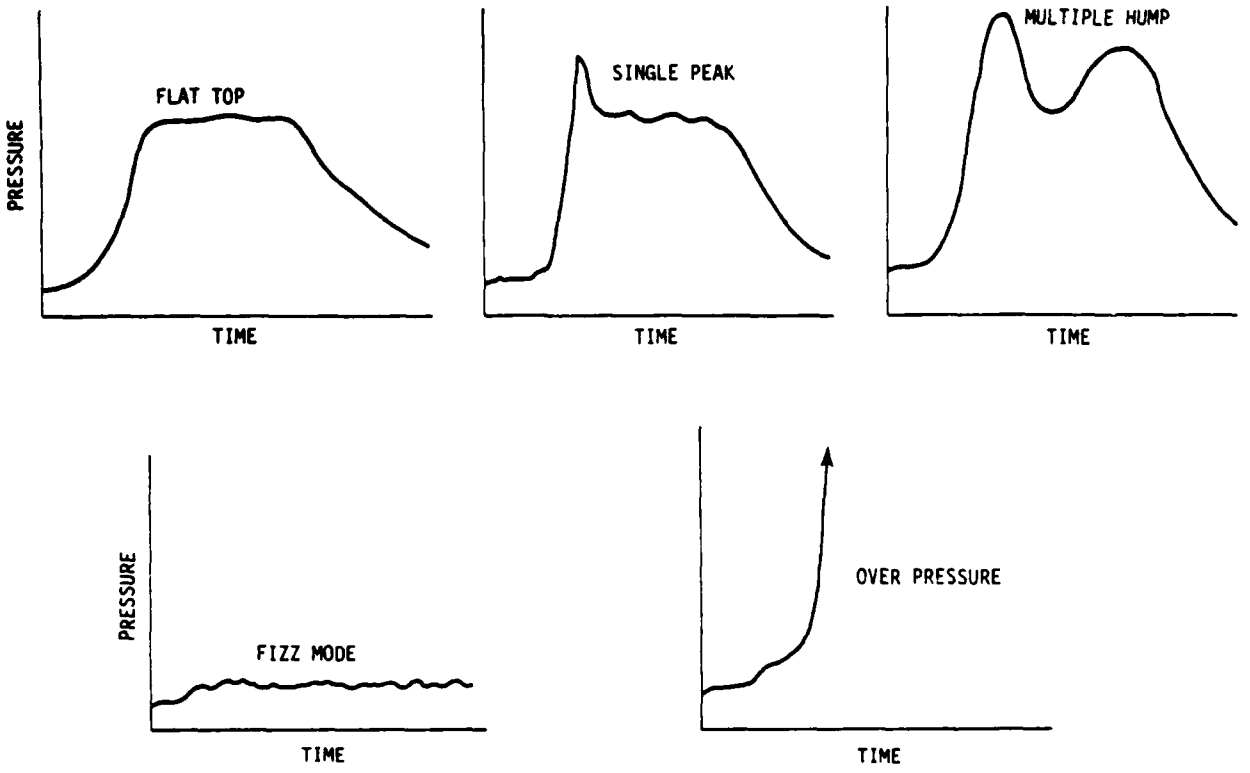

Fig. 1.2. Variability of pressure-time traces - Typical of certain bulk-loaded gun test firings.

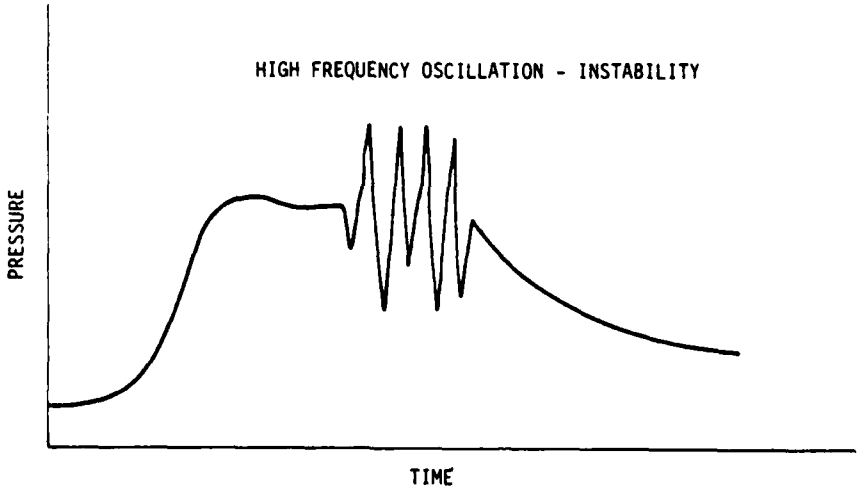

Fig. 1.3. Instability - Typical of certain regenerative-injection gun test firings.

with emphasis on the regeneratively injected gun concept. Prior research on the bulk-loaded gun concept served as a basis for the theoretical work described here. The specific objective was to develop a transient model for the study of flow in the propellant chamber and through orifices. Of particular importance is to establish an understanding of the origin and control of pressure oscillations and the influence of scaling and design features on the combustion process.

In this report, the formulation of a detailed analysis of the transient-flow phenomena that occurs inside the propellant chamber and the injector orifice under conditions typical of LPG operation is described. The effects of orifice channel geometry and wall boundary layer development are included as an inherent part of the transient, two-dimensional framework of governing equations and boundary conditions. The overall interior ballistics analysis utilizes the framework of equations previously developed for the bulk-loaded LPG [1] and generic internal combustion engines [2]. An interior moving boundary accommodates the piston, which is a modification to the original framework [1,2].

The transient orifice flow model was used to parametrically evaluate the sensitivity of the predicted orifice flow phenomena to fluid properties, geometry and operating conditions.

A schematic of regenerative liquid-propellant gun is shown in Fig. 1.4. Existing one-dimensional regenerative LPG analyses involve a number of simplifying assumptions in addition to neglecting multidimensional effects [3-9]. These assumptions relate to such major areas as injection of propellant (treated as a steady-state Bernoulli flow), liquid accumulation in the combustion chamber (either ignored or inferred from experimental data), and fluid flow from the combustion chamber into the gun tube (approximated by steady Bernoulli or isentropic flow). Usually, a number of loss terms are lumped into one or more adjustable discharge coefficients. The veracity of such models to accurately predict the sensitivities of performance to design and operating conditions has not been substantiated. The fundamental coupling of transient flow behavior and physico-chemical processes occuring in the gun chamber is not apparent when the subprocesses are lumped into a single

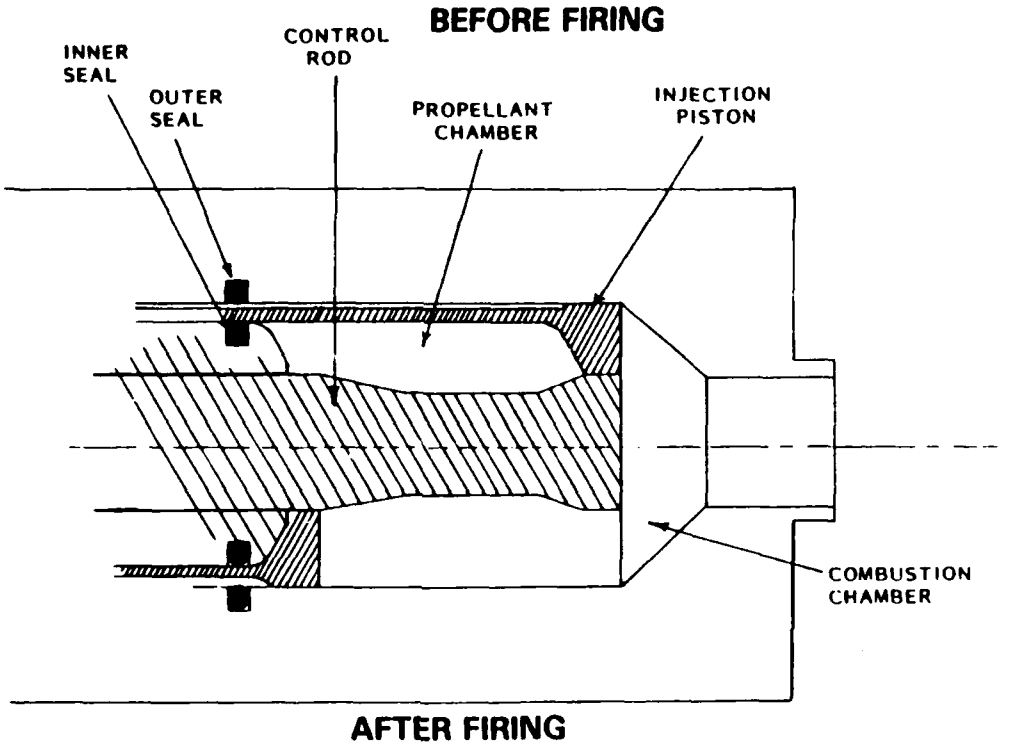

Fig. 1.4. Schematic of a regenerative liquid-propellant gun with an annular piston; reproduced from Ref. [8]

coefficient. Thus, more rigorous modeling of the individual phenomena is needed in order to identify the design parameters most critical to reliable gun performance prediction.

Experiments conducted at the BRL [7], GE [10] and SAIC [11] have used different configurations, piston geometries and piston movements for injecting the liquid through the orifice. A schematic diagram of the configuration is shown in Fig. 1.5 for the three experimental apparatus.

In the present study, the configurations A and B shown in Fig. 1.6 have been studied to establish the adequacy of the transient model for application to the gun problem. Configurations C and D of Fig. 1.6 were not studied due to the termination of the present phase of work.

In Section 2, the formulation and numerical scheme modified for this study are presented. Section 3 presents the results and comparison of predictions with the GE data. Section 4 is comprised of discussion and conclusion.

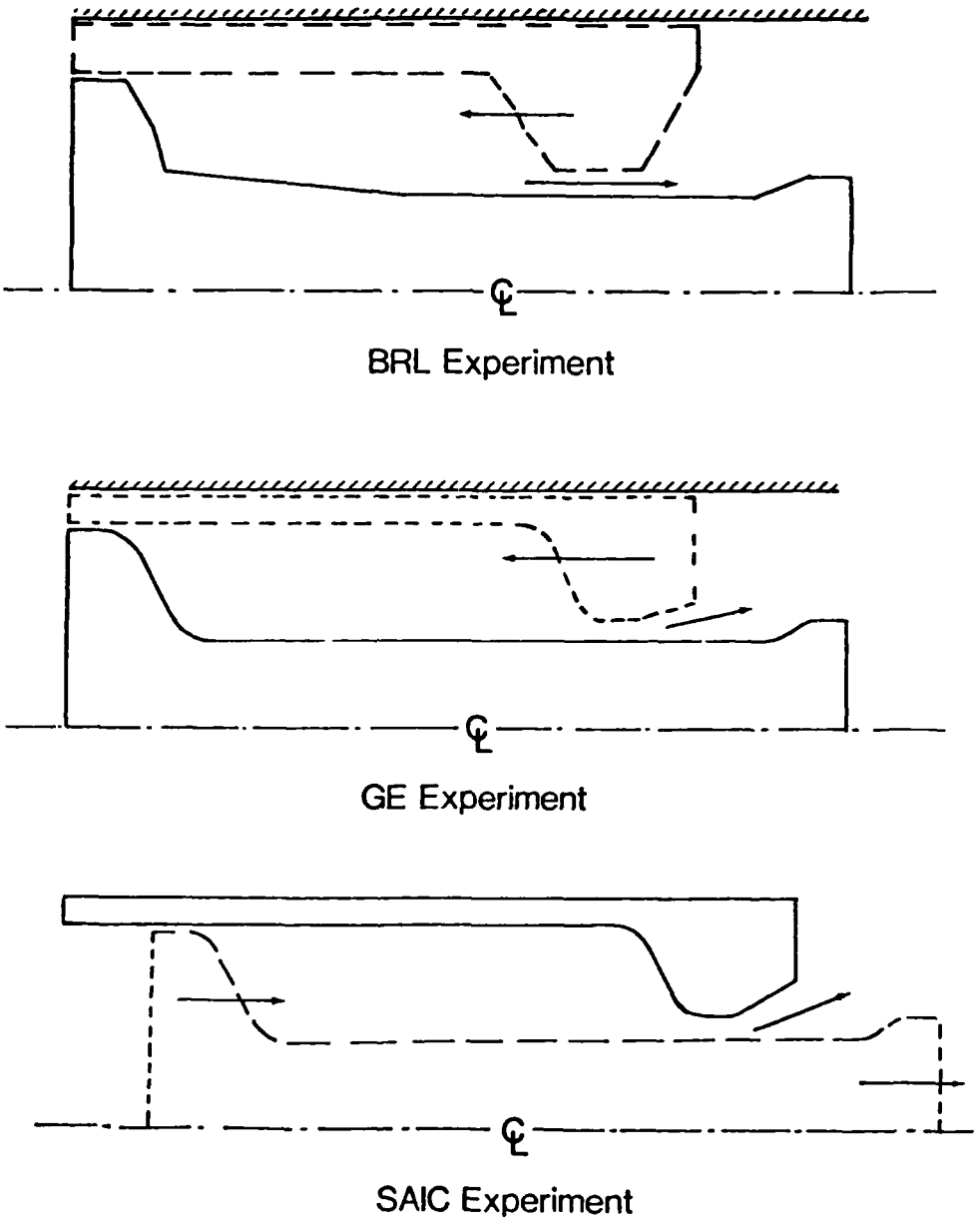

Fig. 1.5. Schematic diagrams of the three experimental configurations.

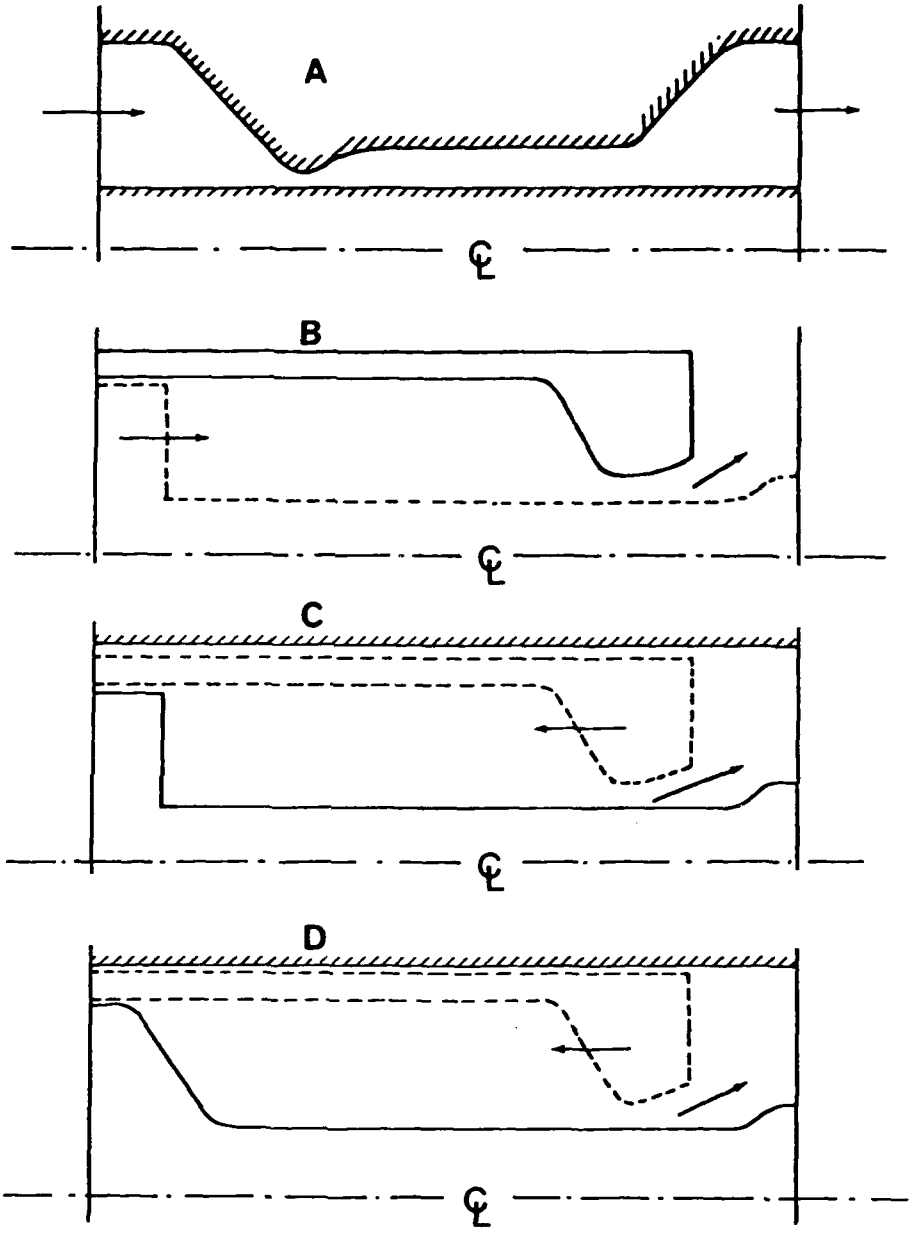

Fig. 1.6. Configurations studied in the present work (A and B) and for future studies (C and D).

2. FORMULATION AND NUMERICAL SCHEME

The computer code is an adaptation of MAGIC (Modeling Algorithm for Generic Internal Combustion Engine) developed over the past ten years [2]. The time-dependent model is two-dimensional (rectangular or axisymmetric) and uses a generalized coordinate system with quadrilateral finite-difference cells for defining general curvilinear cylindrical volumes, in addition to an arbitrary Lagrangian to Eulerian coordinate system for time-dependent in-cylinder boundary definition. MAGIC uses a control-volume differencing scheme with upwind and centered spatial differencing.

The code uses explicit time differencing with semi-implicit time splitting options for acoustic waves, coupled species reaction rates and turbulent production/dissipation rates. It embodies multi-species transport with multi-step hydrocarbon chemistry and/or turbulent reaction-rate closure, with the capability of handling axisymmetric swirling flows with coupled solution for swirl velocity component. Navier-Stokes molecular and turbulent stress as well as thermal and species diffusion are accounted for in addition to compressibility and streamline curvature modifications (see [2] and references cited there).

The chemistry option was not required in the present study, since the focus of attention was on orifice flows. The existing turbulence models are based on steady-state flows, i.e., the models have been developed and calibrated against steady-state data. In addition, in this highly transient flow, there is a basic question of whether the time is sufficient for the flow to become turbulent. Not having the answer to this question, the work reported here is limited to laminar-flow assumption.

The governing equations include the conservation of mass, momentum, energy, and chemical species as well as the thermal and caloric equations of state and appropriate initial and boundary conditions. These equations are described in integral form for a finite-difference grid element which may be in motion with an arbitrary, prescribed velocity $\vec{U}$. This is in accordance with the control-volume differencing approach. For a time-varying volume element V(t) with a surface S(t) and an outward-directed normal vector $\hat{n}$, the governing equations can be written as follows:

Conservation of Mass

$$\frac{\partial}{\partial t}\int_{V(t)} \rho dV - \int_{S(t)} \rho(\vec{U}-\vec{u}) \cdot \hat{n} dS = 0 , \tag{2.1}$$

Conservation of Momentum

$$\frac{\partial}{\partial t}\int_{V(t)} \rho\vec{u} dV - \int_{S(t)} \rho\vec{u}(\vec{U}-\vec{u}) \cdot \hat{n} dS + \int_{S(t)} P\hat{n} dS = \int_{S(t)} \underline{\underline{\tau}}\hat{n} dS , \tag{2.2}$$

Conservation of Energy

$$\frac{\partial}{\partial t}\int_{V(t)} \rho e_T dV - \int_{S(t)} \rho e_T(\vec{U}-\vec{u}) \cdot \hat{n} dS + \int_{S(t)} (\hat{n} \cdot \vec{u}) P ds = \int_{S(t)} \hat{n} \cdot \vec{u}\underline{\underline{\tau}} dS + \int_{S(t)} \hat{n} \cdot \left(\sum_i e_i \vec{J}_i\right) dS + \int_{S(t)} \hat{n} \cdot \vec{q}\, dS , \tag{2.3}$$

Conservation of Species

$$\frac{\partial}{\partial t}\int_{V(t)} \rho F_i dV - \int_{S(t)} F_i(\vec{U}-\vec{u}) \cdot \hat{n} dS = \int_{V(t)} \langle \dot{\rho}_i \rangle dv + \int_{S(t)} \hat{n} \cdot \vec{J}_i \, dS , \tag{2.4}$$

where ρ = fluid density, $\vec{u}$ = fluid velocity, e_T = specific total energy, U = grid velocity, P = pressure, $\vec{q}$ = heat flux vector, T = temperature, $e_i(T)$ = specific internal energy of specie i including the energy of formation, $\vec{j}_i$ = diffusion flux vector for specie i, and F_i = mass fraction of specie i, with $\sum_i F_i = 1$ and $\rho_i = \rho F_i$. The stress tensor, $\underline{\underline{\tau}}$, is assumed to include both laminar and turbulent contributions within an eddy viscosity formulation, for turbulent-flow applications (see the references cited in [2]).

Currently, the model includes provisions for defining the gas-phase pressure as a mixture of ideal gases as given by:

$$P = \sum_i \rho_i \frac{\hat{R}}{M_i} T \,, \tag{2.5}$$

where R is the universal gas constant and M_i is the species molecular weight. The caloric equation of state may be written as:

$$\left.\begin{aligned} e &= \sum_i \rho_i e_i \\ e_i &= a_i T + b_i T^2 + e_{i,o} \,, \end{aligned}\right\} \tag{2.6}$$

where e is the mixture specific internal energy, e_i is the internal energy of the gaseous specie i, and a_i, b_i, and $e_{i,o}$ are constants. All constants in the caloric equation of state are correlated from the thermodynamic data available in JANAF tables for the species of interest.

The model equations may be solved in one or two spatial dimensions with a generalized mesh which may move with time and an acoustically implicit solution for the pressure. The finite-difference grid of general quadrilateral cells are conformal to solid surfaces. The generalized mesh allows the grid points to move with the fluid (Lagrangian), be held fixed (Eulerian) or move in a prescribed manner (e.g., due to a moving solid boundary). The staggered grid system uses cell-centered scalar quantities and node-centered flow velocities (Fig. 2.1). Explicit time differencing and centered spatial differencing are

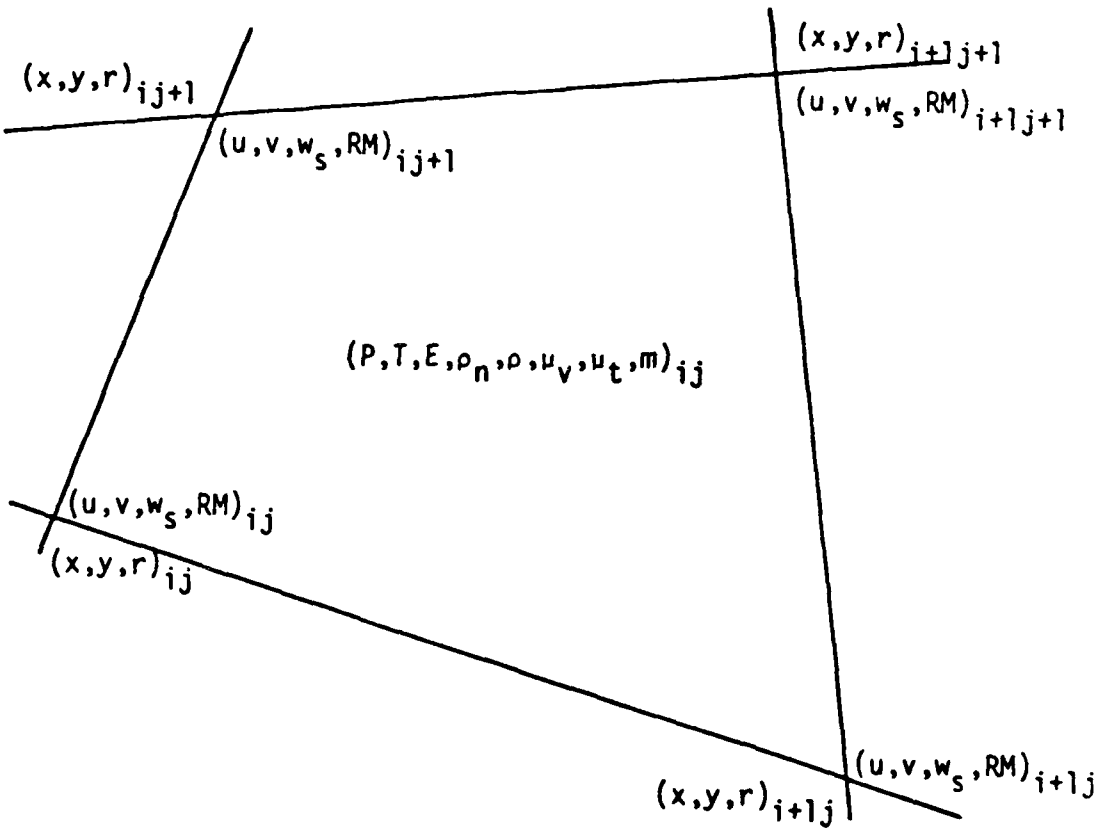

Fig. 2.1. General quadrilateral computational cell; reproduced from Ref. [2].

used for the stress terms. The system of finite-difference equations is solved by explicit time integration beginning from a set of initial conditions, and using separate steps for various terms in the conservation equations. This is accomplished by updating the velocities and energy to an intermediate step accounting for pressure forces and stresses. An acoustic implicitization technique is then used in order to overcome the courant restriction (due to the use of explicit technique), i.e., the computational time step being less than the time it takes an acoustic wave to propagate across a computational zone, which severely restricts the time step due to the large difference between the flow speeds and the local sound speed. Finally, the advection terms are solved, rezone is performed, and (if appropriate) the chemical reactions are computed, completing the computational cycle. The grid points are then moved to their next time level and the flow quantities are updated, accounting for thermal and species diffusion using centered differencing of the diffusion terms. The entire procedure is then repeated to advance the solution in time. A complete description of the model and numerical scheme is given in Ref. [2].

3. RESULTS

The transient, two-dimensional (axisymmetric) analysis was applied to different geometries and problems in order to identify and address the important fundamental processes that occur during the injection of liquid propellants in typical gun configurations with moving boundaries. This modular model was applied to the propellant chamber and the injector. The modular approach, in which the model is first applied separately to each of the major components of the gun provides advantages (numerically) both in dealing with the wide range of time and spatial scales of the problem and in isolating each of the major processes for detailed study. The dearth of information on the flow phenomena occuring inside orifices and injectors in general, and under transient conditions in particular, coupled with the emerging evidence that this internal flow behavior affects the spray combustion process, has led to the current focus of research on this process.

The computer model was first applied to the case of a laminar flow of a liquid through a straight cylindrical annulus where an analytical solution exists. The velocity distribution for steady, incompressible flow in an annulus is

$$v = \frac{(P_o - P_L)R^2}{4\,\mu\,L}\left[1 - \left(\frac{r}{R}\right)^2 + \left(\frac{1 - k^2}{\ell n(1/k)}\right)\ell n\left(\frac{r}{R}\right)\right], \qquad (3.1)$$

where v is the velocity, P_o and P_L are the pressures at the inlet and exit planes of the annular tube of length L, μ is the viscosity, R is the outer-tube radius, kR is the inner-tube radius, and r is the radial location with respect to the centerline of the geometry.

The transient code was applied to the flow of a liquid in a cylindrical annulus, and the velocity distribution was compared to the results of the analytical solution once the transient model approached steady state. Figure 3.1 shows the comparison between the prediction and the analytical solution,

indicating that the model is capable of predicting this type of flow. The sensitivity of the predictions to grid size, i.e., numerical diffusion effects, is shown in Fig. 3.2. The issue of numerical diffusion will be addressed later in this report.

In order to identify the sensitivity of the flow structure to the orifice geometry, theoretical predictions were carried out for the flow of a liquid through two annular orifices, each having a different contour along its length. In one, the cross section was constant (Case 1), while in the other, a minimum section was placed near the entrance to the orifice (Case 2). The computational mesh, velocity vectors and fluid speed contours are shown in Fig. 3.3 for the constant cross-section orifice and in Fig. 3.4 for the orifice with a minimum cross section at the entrance. Each figure gives the theoretical predictions for three different times. The propellant and combustion chambers have radii of 1.5 cm and lengths of 2 cm. The annular region in both cases is 1.5 cm long. The width of the annulus is 0.15 cm in case 1 (straight channel). The annulus in case 2 has a width of 0.30 cm in general, but it narrows down to a width of 0.15 cm at the propellant chamber. The grids do not move during this calculation. The time-dependent pressure boundary conditions are shown in Fig. 3.5. The imposed pressure difference causes the propellant to flow through the annulus from the propellant chamber to the combustion chamber. Figure 3.6 shows the pressure profiles for different times at the right-hand-side boundaries of cases 1 and 2. The plots show that both calculations come to a near-steady state after approximately 1 msec.

The profiles of pressure at the end of calculation (1.14 msec) are compared in Fig. 3.7. It can be seen that in the straight orifice (Case 1), the pressure decreases linearly along the length, whereas in Case 2 (orifice with a minimum section at the inlet), the pressure falls to a minimum at the minimum section and then increases as the combustion chamber is approached.

The predictions of the velocity vectors shown in Figs. 3.3 and 3.4 indicate that the flow structure is extremely sensitive to the orifice contour. The straight orifice prediction (Fig. 3.3) shows the development of a recirculation zone downstream of the orifice exit. As can be seen in Figs. 3.3(a)-(c), this recirculation zone increases in size with time and expands into the exit plane

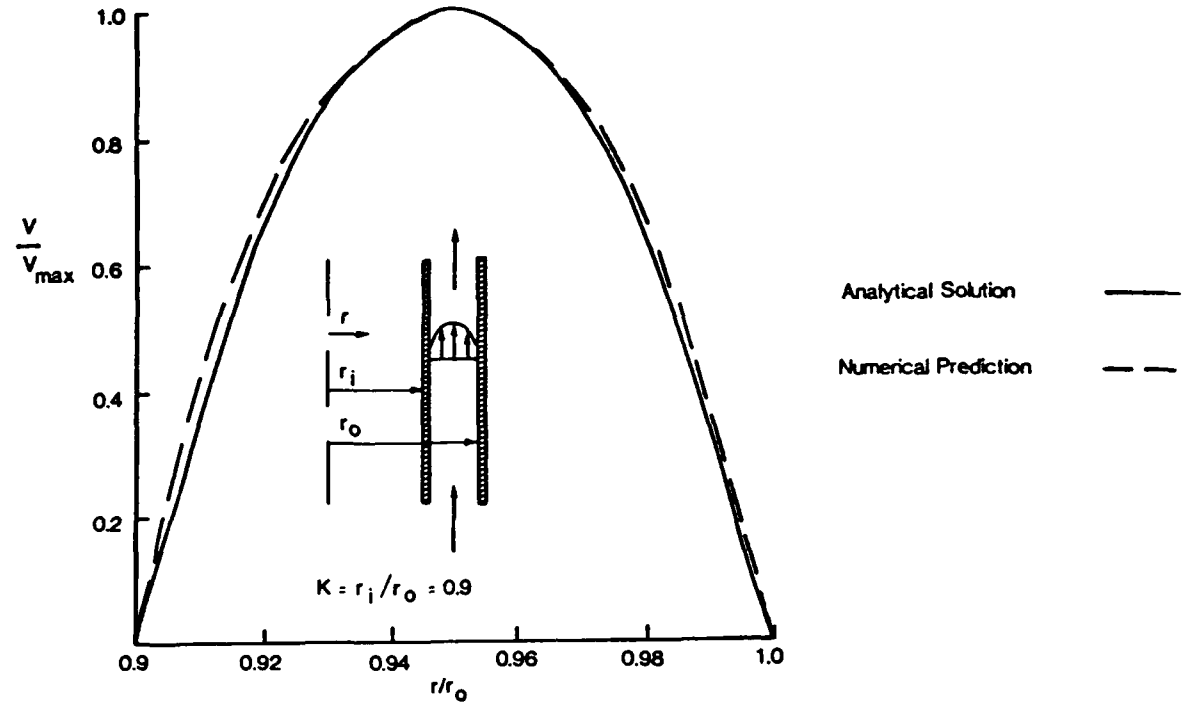

Fig. 3.1. Comparison between the prediction and analytical solution for the flow of a liquid in a straight, cylindrical annulus.

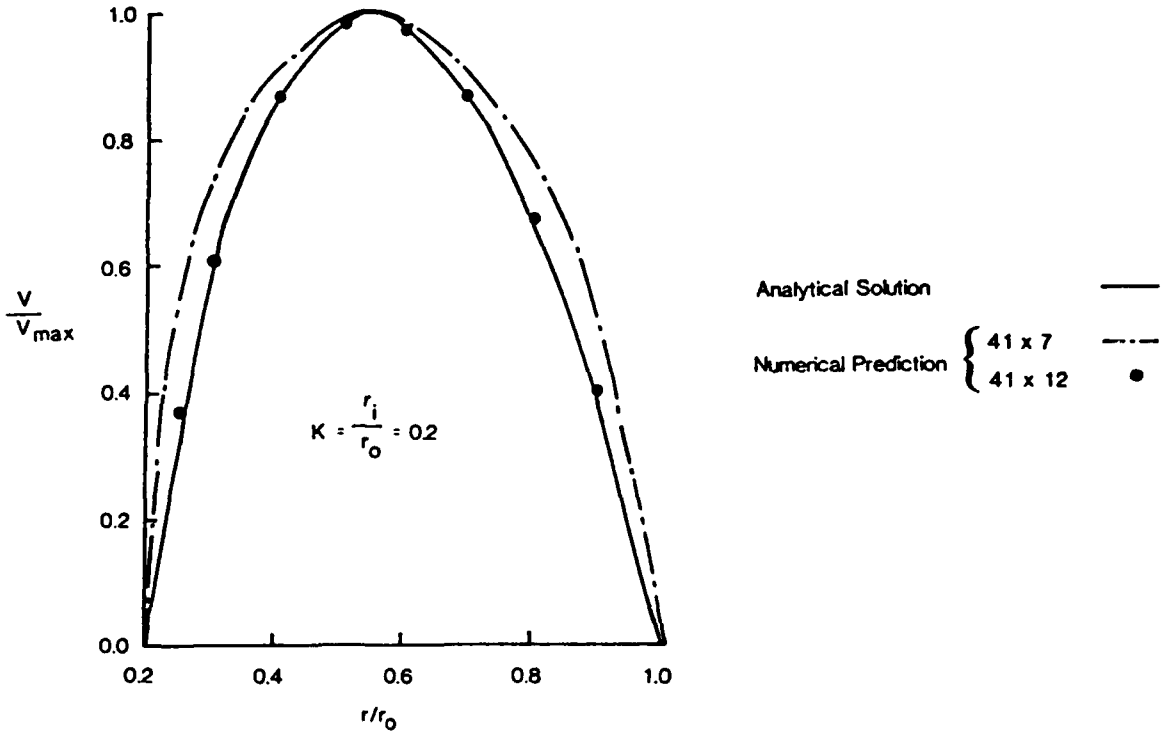

Fig. 3.2. Grid dependency test for the flow of a liquid in a straight, cylindrical annulus.

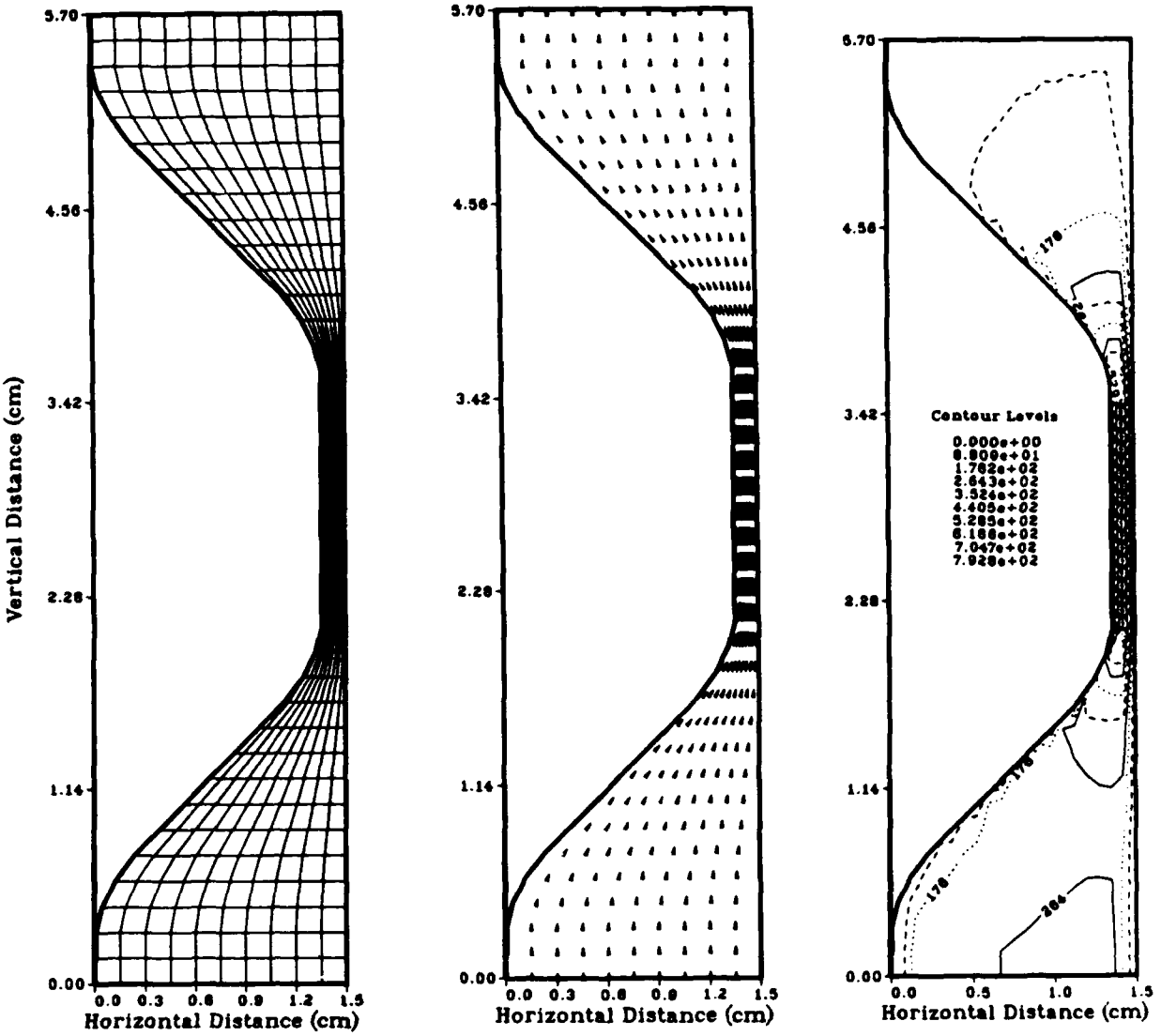

Computational Mesh

Velocity Vectors

Fluid Speed Contours (cm/s)

Fig. 3.3(a). Theoretical predictions for the flow of a liquid through a constant cross-section orifice at t = 0.07 msec.

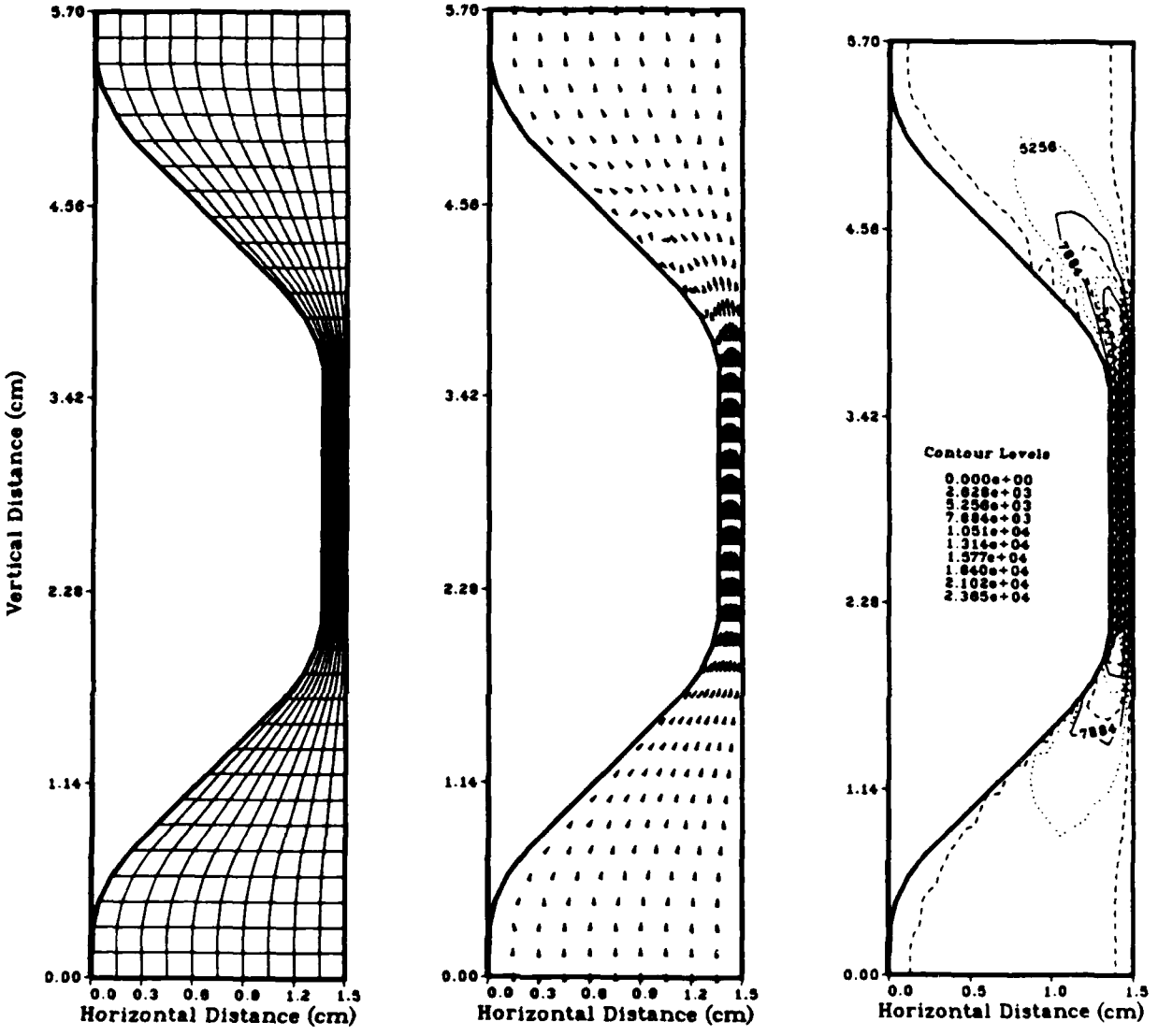

Fig. 3.3(b). Theoretical predictions for the flow of a liquid through a constant cross-section orifice at t = 0.51 msec.

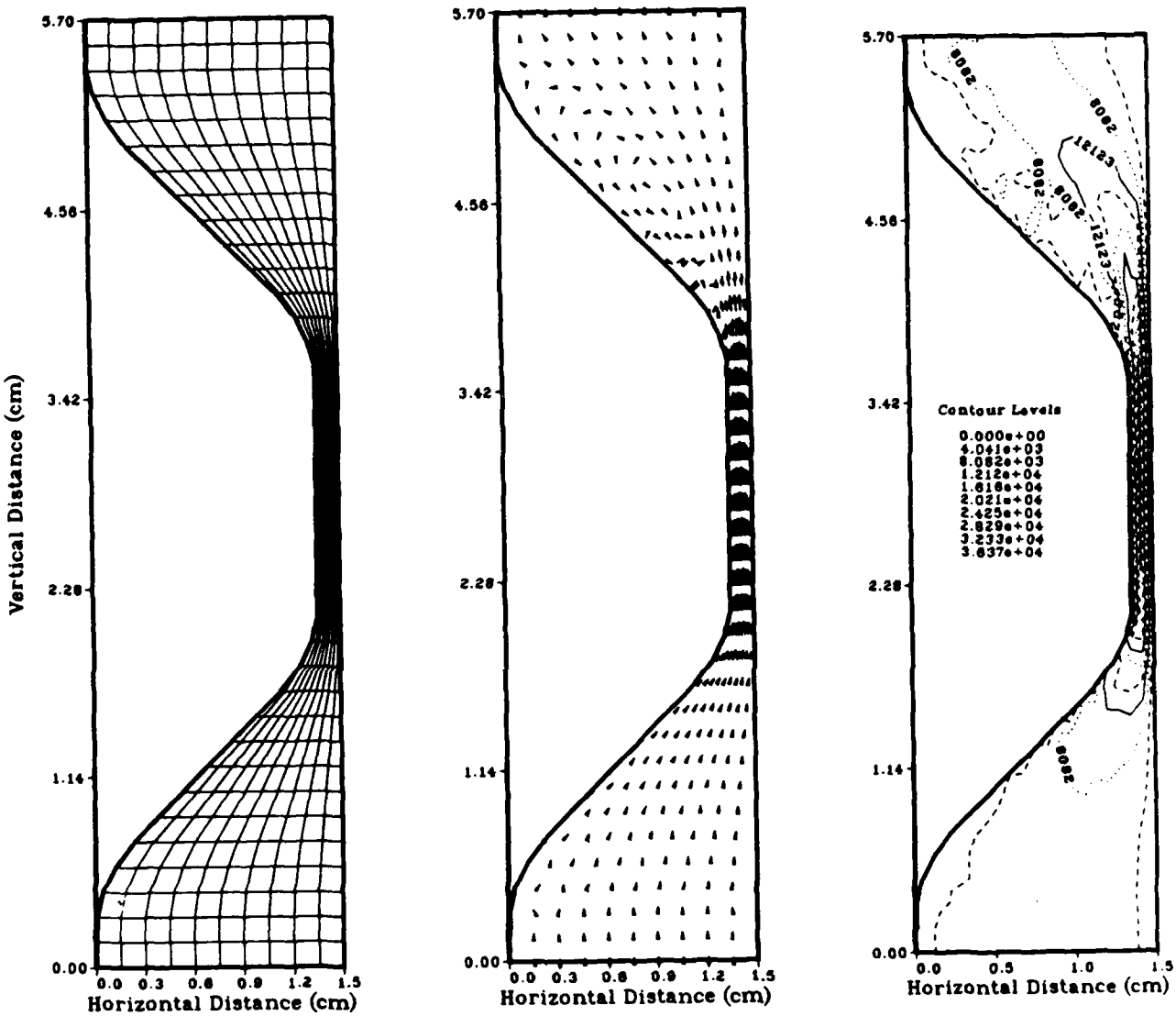

Computational Mesh

Velocity Vectors

Fluid Speed Contours (cm/s)

Fig. 3.3(c). Theoretical predictions for the flow of a liquid through a constant cross-section orifice at t = 1.14 msec.

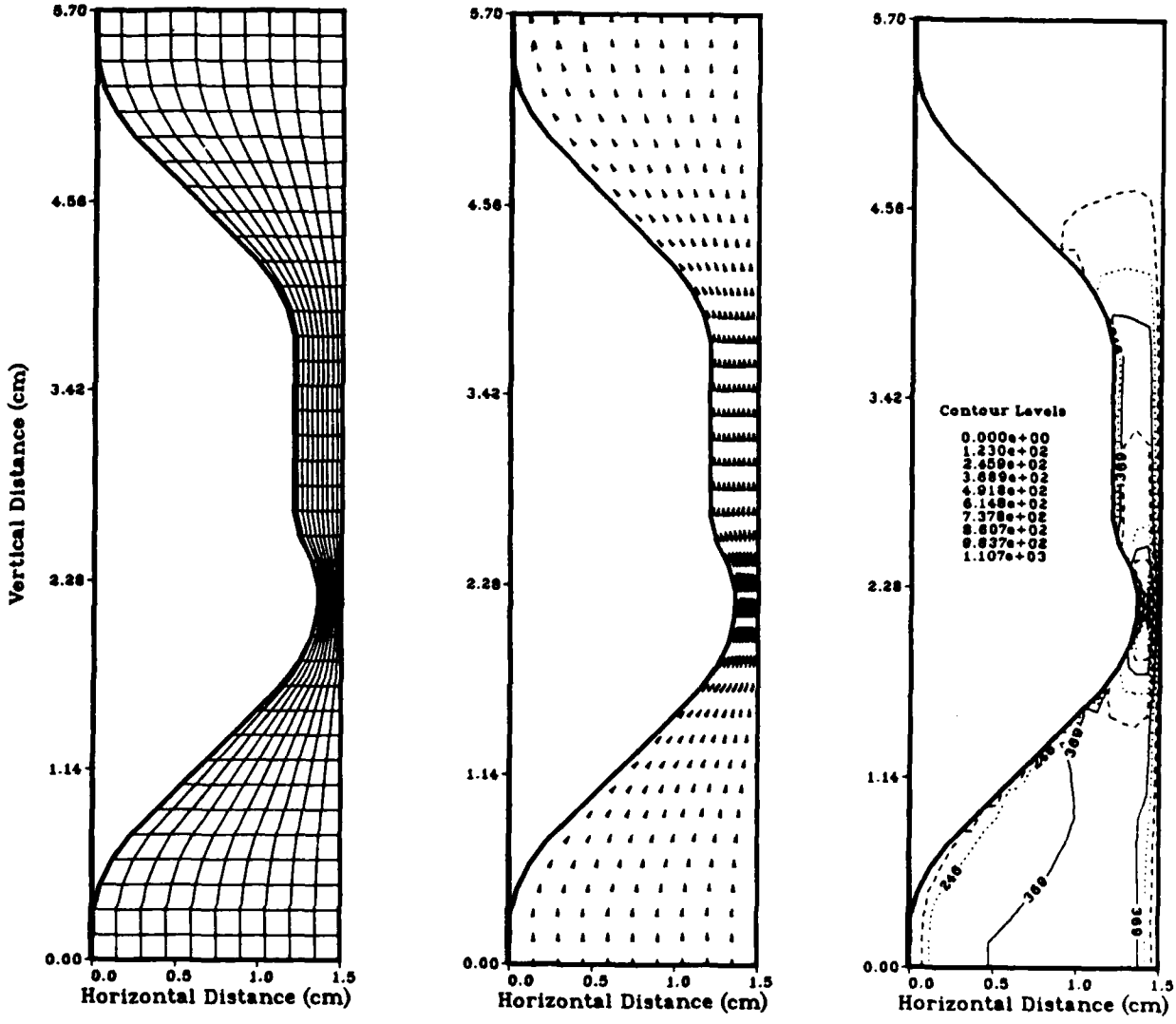

Computational Mesh

Velocity Vectors

Fluid Speed Contours (cm/s)

Fig. 3.4(a). Theoretical predictions for the flow of a liquid through an orifice with a minimum cross-section at the entrance at t = 0.07 msec.

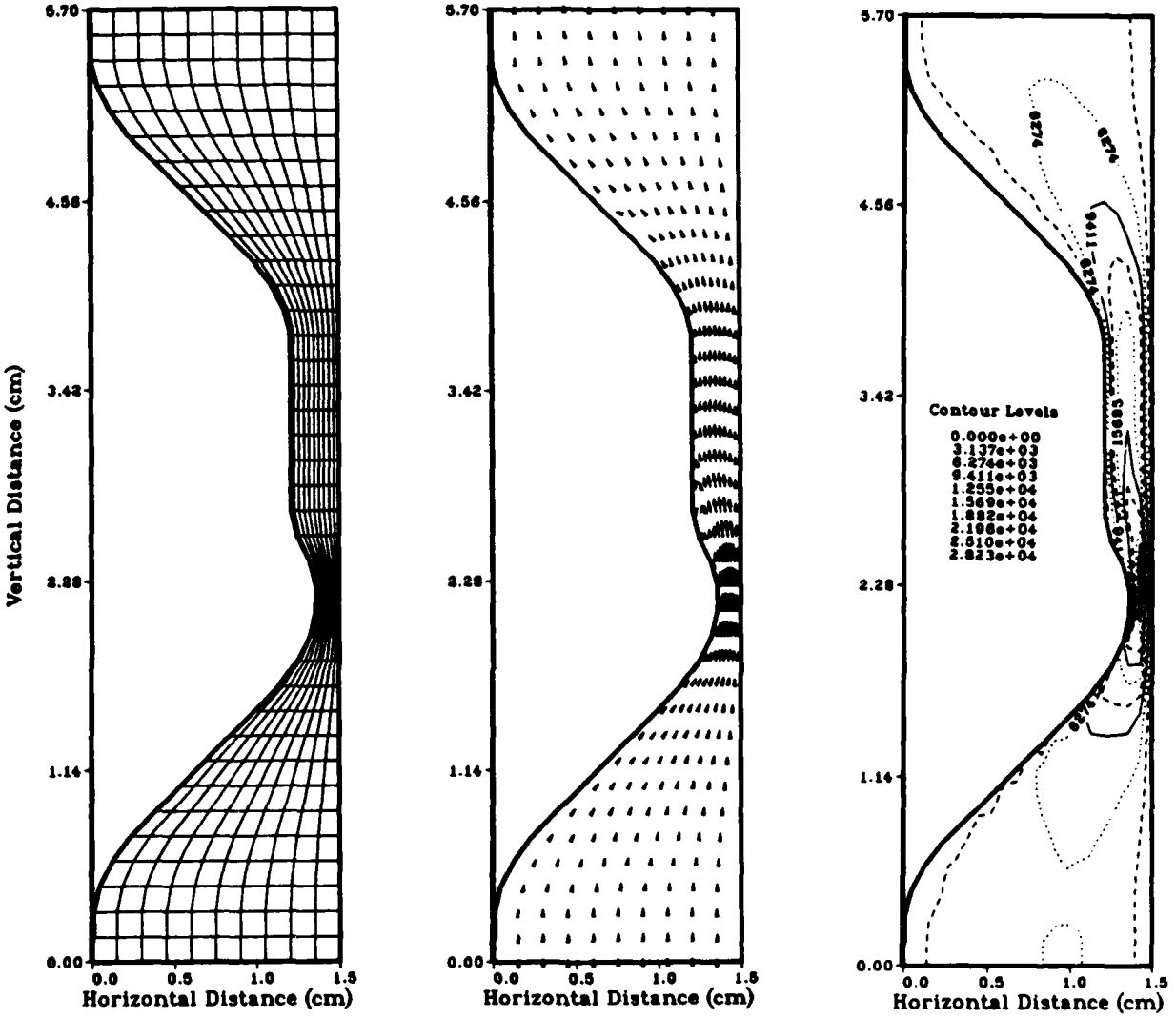

Computational Mesh

Velocity Vectors

Fluid Speed Contours (cm/s)

Fig. 3.4(b). Theoretical predictions for the flow of a liquid through an orifice with a minimum cross-section at the entrance at t = 0.51 msec.

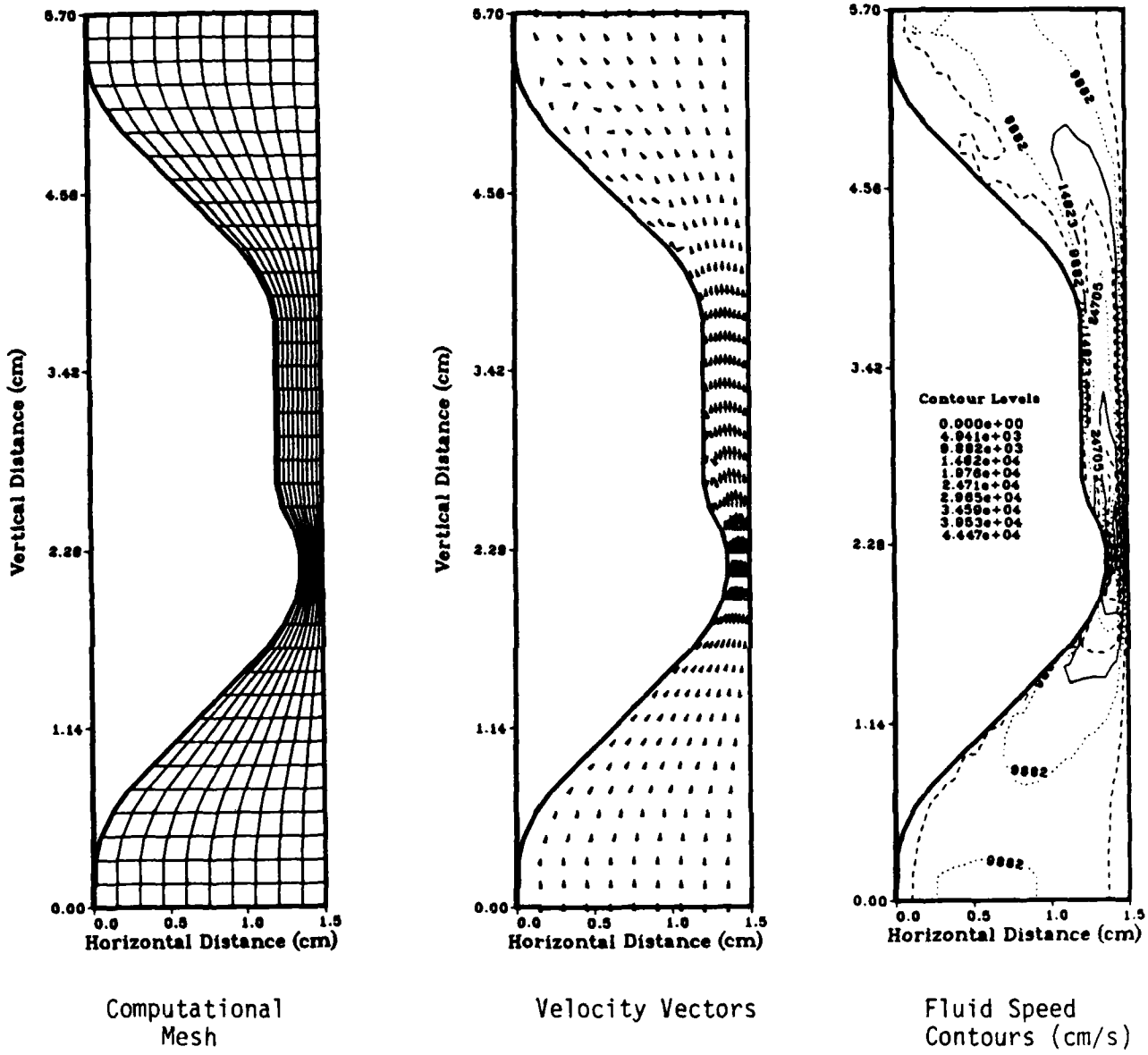

Computational Mesh

Velocity Vectors

Fluid Speed Contours (cm/s)

Fig. 3.4(c). theoretical predictions for the flow of a liquid through an orifice with a minimum cross-section at the entrance at t = 1.14 msec.

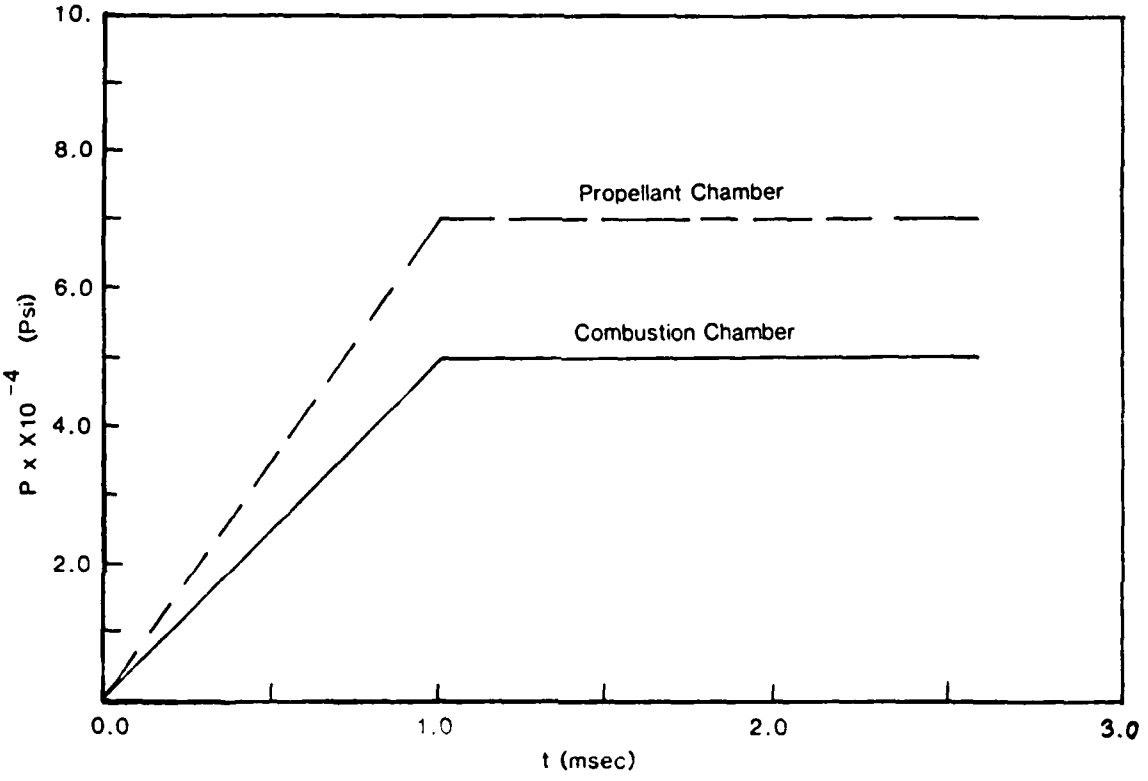

Fig. 3.5. Pressure boundary conditions for the propellant and combustion chambers for Cases 1 and 2 (Figs. 3.3 and 3.4, respectively).

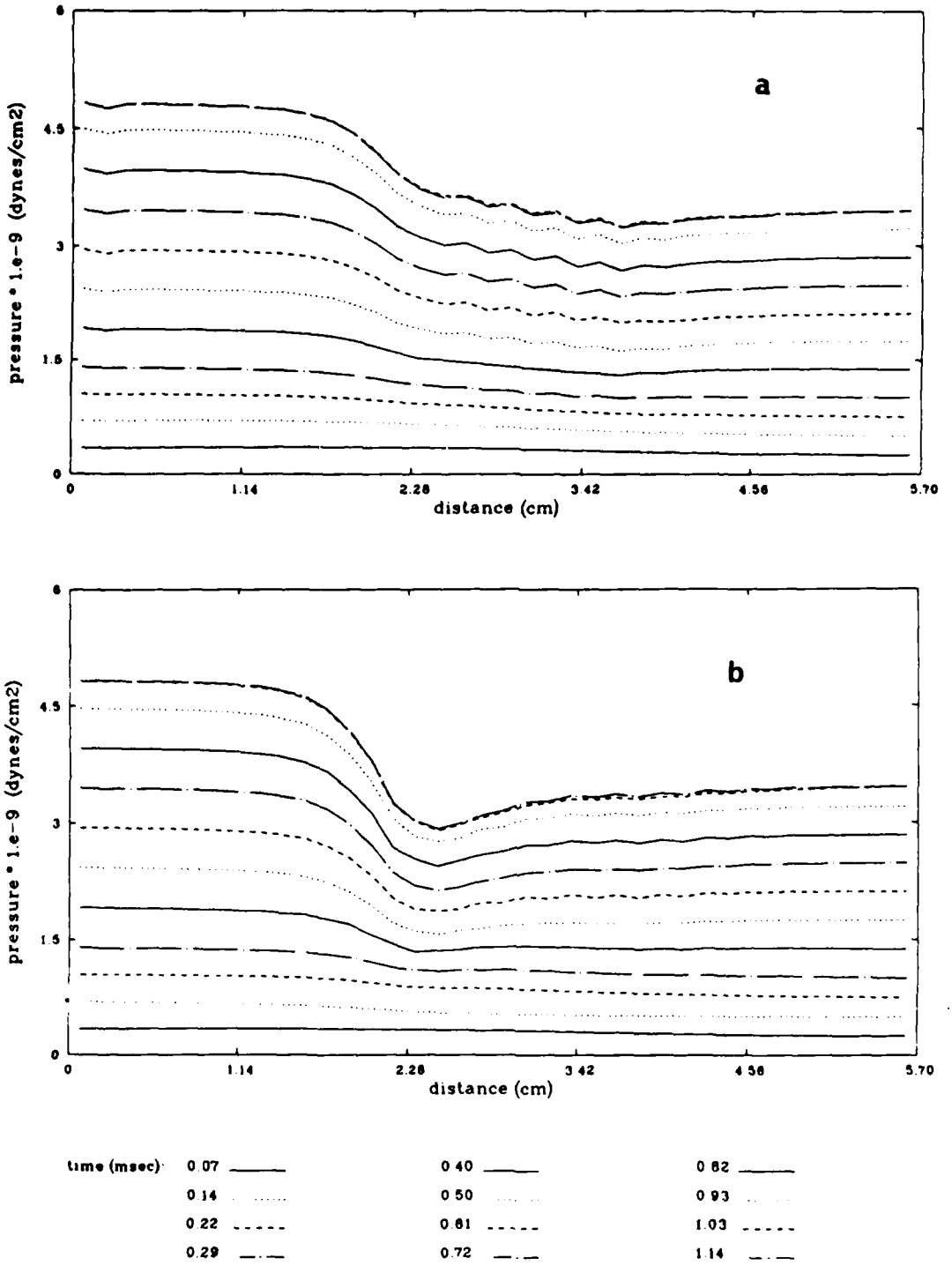

Fig. 3.6. Pressure profiles for (a) straight orifice, i.e., Case 1, and (b) orifice with a minimum cross-section at the entrance, i.e., Case 2. These profiles are plotted for the right-hand-side boundary of the geometries shown in Figs. 3.3 and 3.4, respectively.

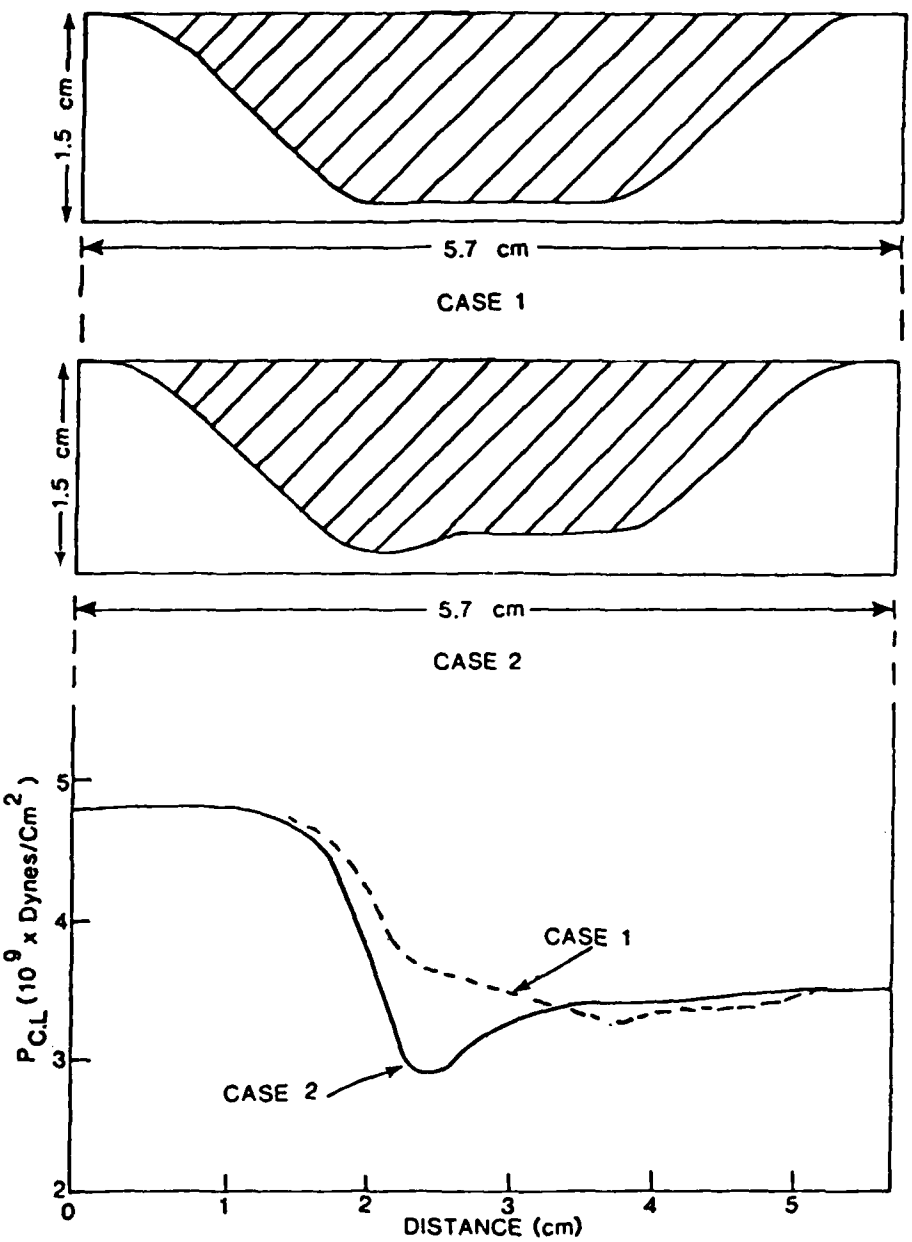

Fig. 3.7. Pressure variation at t = 1.14 msec along the lower boundary of straight orifice (Case 1) and orifice with a minimum section (Case 2).

of the orifice. In the case of the orifice with a minimum section near the entrance, i.e., Figs. 3.4(a)-(c), a similar recirculation-zone behavior can be observed in the vicinity of the exit plane. However, a second recirculation zone develops immediately downstream of the minimum section and it too grows in size with time. Furthermore, conditions may be found where vortex roll-up in the propellant chamber may occur, which will be discussed later. These results appear to be the first detailed orifice calculations made for a liquid undergoing transient flow that take into account the viscous, multi-dimensional flow details. The significance of these results is the predicted sensitivity of the flow structure to the orifice geometry which can be expected to have marked effects on the spray formation and combustion processes. In addition, the development of recirculation zones indicates the potential for the separated-flow region to spread back to the propellant chamber with the possibility that pre-ignition and sporadic combustion might occur. The prediction of these phenomena not only depend on accounting for transient-flow development, but are critically dependent on the two-dimensional nature of the flow.

The discharge coefficient, defined as

$$C_D = \dot{m}_{actual} / \dot{m}_{theoretical} \quad , \tag{3.2}$$

where $\dot{m}$ is the mass flow rate, with $\dot{m}_{theoretical}$ being calculated from steady, 1-D calculations, is plotted in Fig. 3.8 for Cases 1 and 2. Later, the discharge-coefficient calculations and results for the moving-piston case and comparisons with the GE results will be presented.

The GE configuration shown in Fig. 1.5 was not used due to the complexity of the geometry and rezoning required in the present phase of the effort. Instead, the geometry shown in Fig. 3.9 was used with the flat piston moving in the opposite direction of the GE piston movement. However, grid movement (i.e., variation of the domain of integration with respect to time due to the piston movement) was incorporated in the computer model in the uniform-area section of the propellant chamber. The following experimental data for the quasi-steady discharge coefficients in annular orifices were among those provided by GE [10] which were selected for comparisons with the predicted

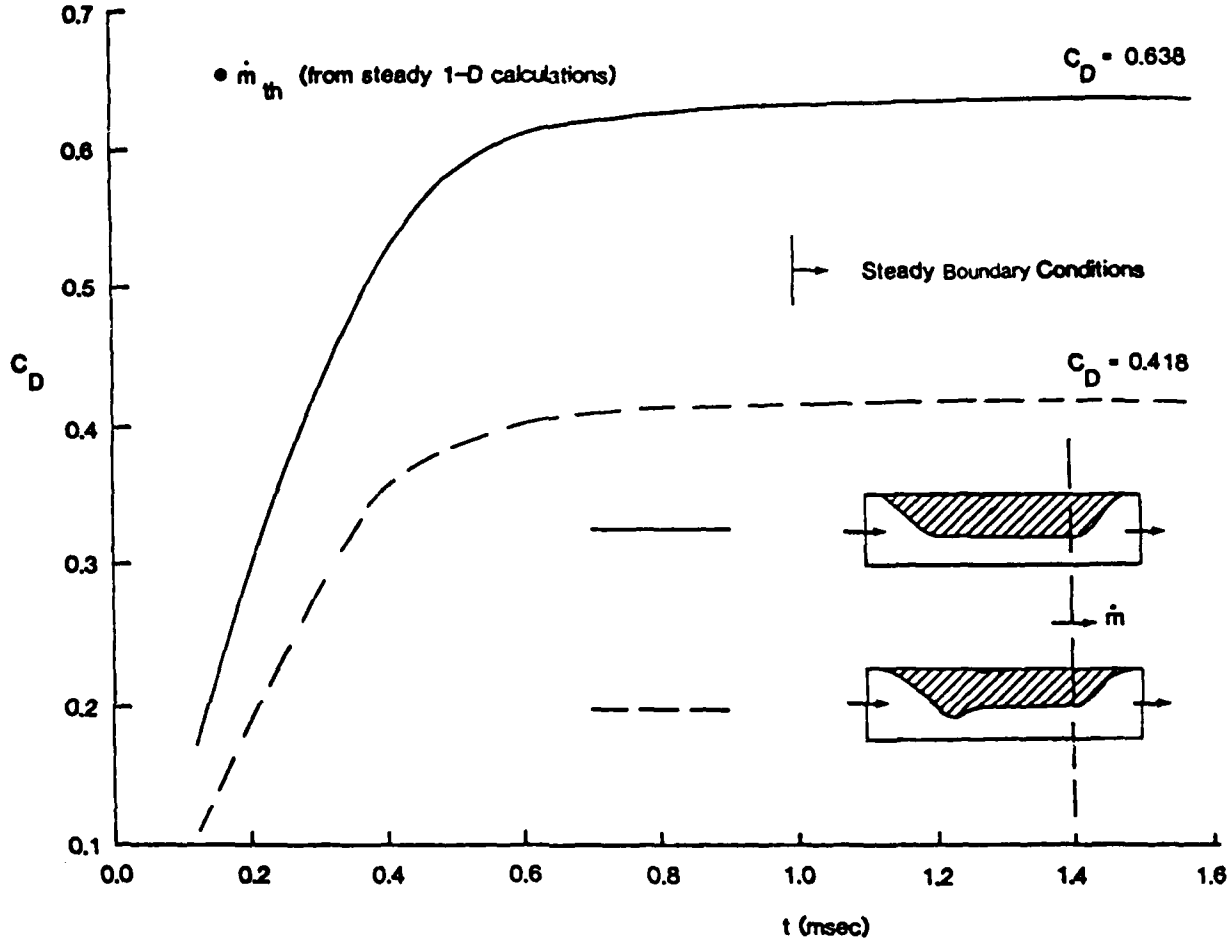

Fig. 3.8. Variation of discharge coefficient with time for Cases 1 and 2 of Figs. 3.3-3.7.

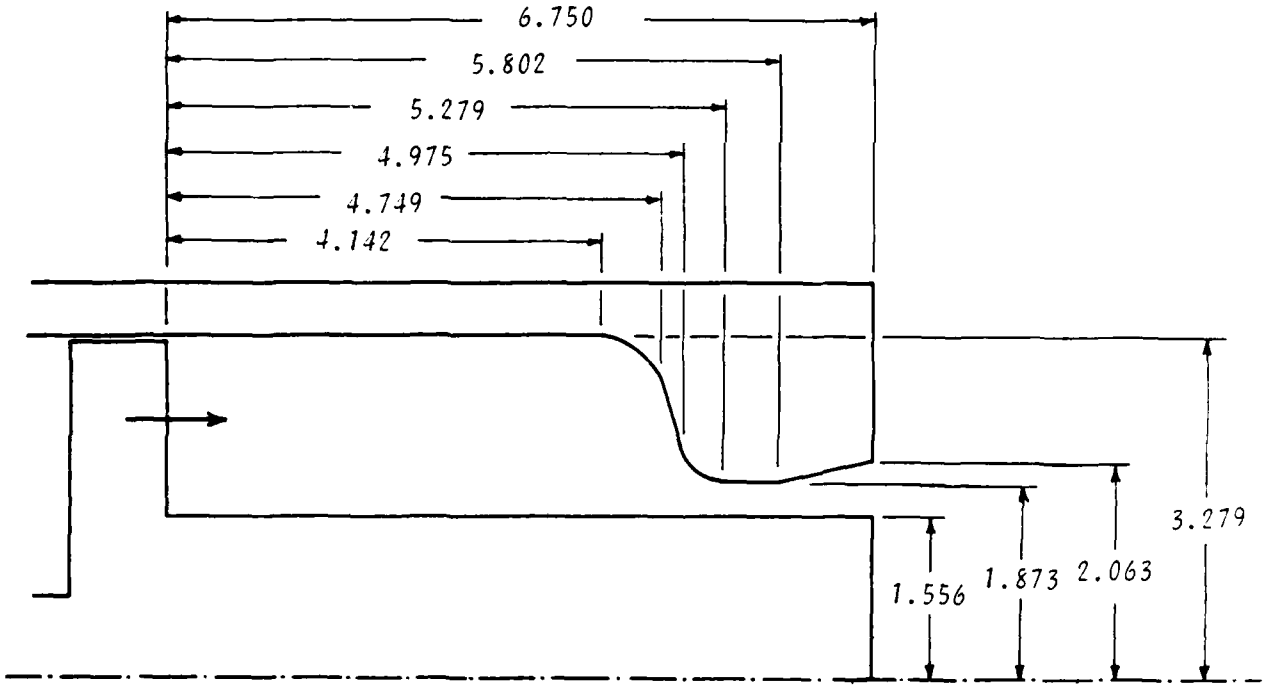

Fig. 3.9. The moving-piston geometry used in the present study; dimensions are in cm.

discharge coefficients:

Test No.	Gap(in.)	P_C(Psi)	P_L(Psi)	T(Ĉ)	μ(cp)	V_p(in./sec)	C_D
1	0.125	1239	1763	15	9	389	0.99
10	0.125	1247	1774	- 8	23.5	370	0.94
20	0.125	1078	1534	-28	78	288	0.79
27	0.125	1815	2582	-37	175	300	0.64

Note that the values of C_D were corrected for calculating the area of the flow used in the calculation of volume-flow rate and fluid pressure adjacent to the piston. These corrections were communicated to GE staff conducting these cold-flow studies. Here, the gap distance of 0.125 in. is the minimum section in the orifice (Fig. 3.9), P_C is the combustion-chamber pressure measured when the piston velocity becomes constant, P_L is the liquid-propellant pressure, T is the propellant temperature, μ is the propellant viscosity, and V_p is the piston velocity.

The discharge coefficient obtained from the predictions was based on the following formula:

$$C_D = \frac{Q_{actual}}{Q_{theoretical}} = \frac{Q_{actual}}{A_2\, v_{th.}} = \frac{Q_{actual}}{A_2\sqrt{\dfrac{2\Delta P}{\rho\,(1 - A_2^2/A_1^2)}}}\,, \qquad (3.3)$$

where Q is the volume-flow rate, A_1 is the piston area, A_2 is the minimum gap area, ρ is the propellant density (assumed constant), ΔP is the pressure difference between the piston face and the orifice minimum area, and v_{th} is the theoretical velocity obtained from the Bernoulli equation. Q_{actual} was calculated in the code from the integration of $\bar{v}.\Delta A$ across the piston face, where $\bar{v}$ is the average fluid velocity between two adjacent grid points.

Comparisons of the discharge coefficients obtained from the data and the computer code are shown in Fig. 3.10 as a function of propellant temperature.

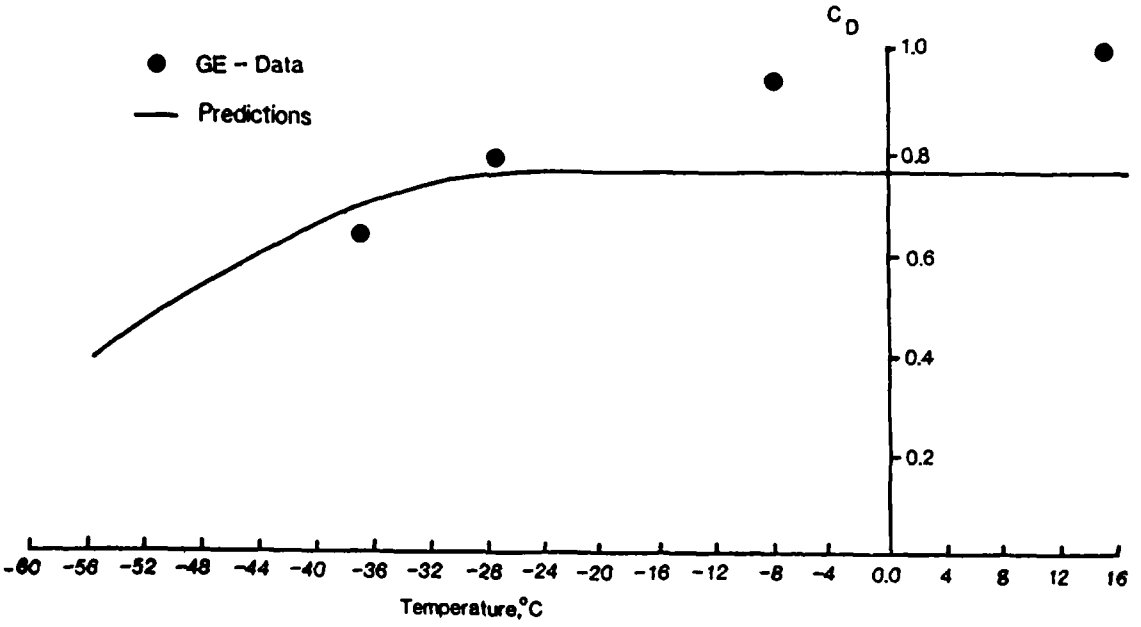

Fig. 3.10. Comparisons between the predicted and measured discharge coefficients.

The agreement between the predictions and C_D data appear good at relatively low temperatures where the viscosity of the liquid propellant is relatively high. However, for higher temperatures and consequently smaller viscosities, the disagreement between the predictions and data is significant. Moreover, the predictions are almost flat for temperatures greater than -24 °C which suggests that numerical viscosity (which will be discussed later) is greater than the physical viscosity.

Figures 3.11(a)-(j) show the grid distributions and velocity-vector plots for 0.4, 0.8, 1.2, 1.6, 2.0, 2.4, 2.8, and 3.2 msec for Run No. 1 of GE with T = 15 °C, μ = 9 cp, V_p = 389 in./sec, and P_c = 1239 psi. The flow is well-behaved through the main chamber, the convergent section, the orifice, and the divergent exit, with the exception of development of some non-uniformities in two regions, one at the beginning of the converging section in the vicinity of the fixed wall and one in the upper corner between the piston face and the fixed wall. The non-uniformities developed at the upper corner of the piston face exist at all times; they smoothen themselves in the axial direction, but propagate in the radial direction with time. Those developed at the entrance to the converging section (or, in other words, the beginning of the fixed-grid zone at x = 3.5 cm) do not appear until times of approximately 1.6 msec, see Fig. 3.11(d). The disturbances at the converging wall and those at the piston/wall region do not appear to be of the same origin, although they share the same physical explanation, i.e., the no-slip condition at the wall and a relatively coarse mesh for the treatment of the developing boundary layer. Those non-uniformities originating at the piston/wall corner may be attributable to the tendency of a vortex roll-up process developed due to scrubbing of the fluid by the piston moving along the fixed wall. This is a hypothesis which needs further study to verify. The disturbances developed at the converging wall can be explained in terms of the aspect ratios of the individual cells and the ratio of the sizes of the last moving grid and the first fixed grid (at x = 3.5 cm) which exceeds the allowable limits of 0.8-1.2 (see Ref. [2]) as is seen in Fig. 3.11(d). Clearly, the cause of this behavior is a combination of large cell aspect ratios in the regions of steep gradients and the shrinking of the moving-grid cells which result in the ratio of adjacent grid sizes at the boundary of the moving-grid zone and the fixed-grid

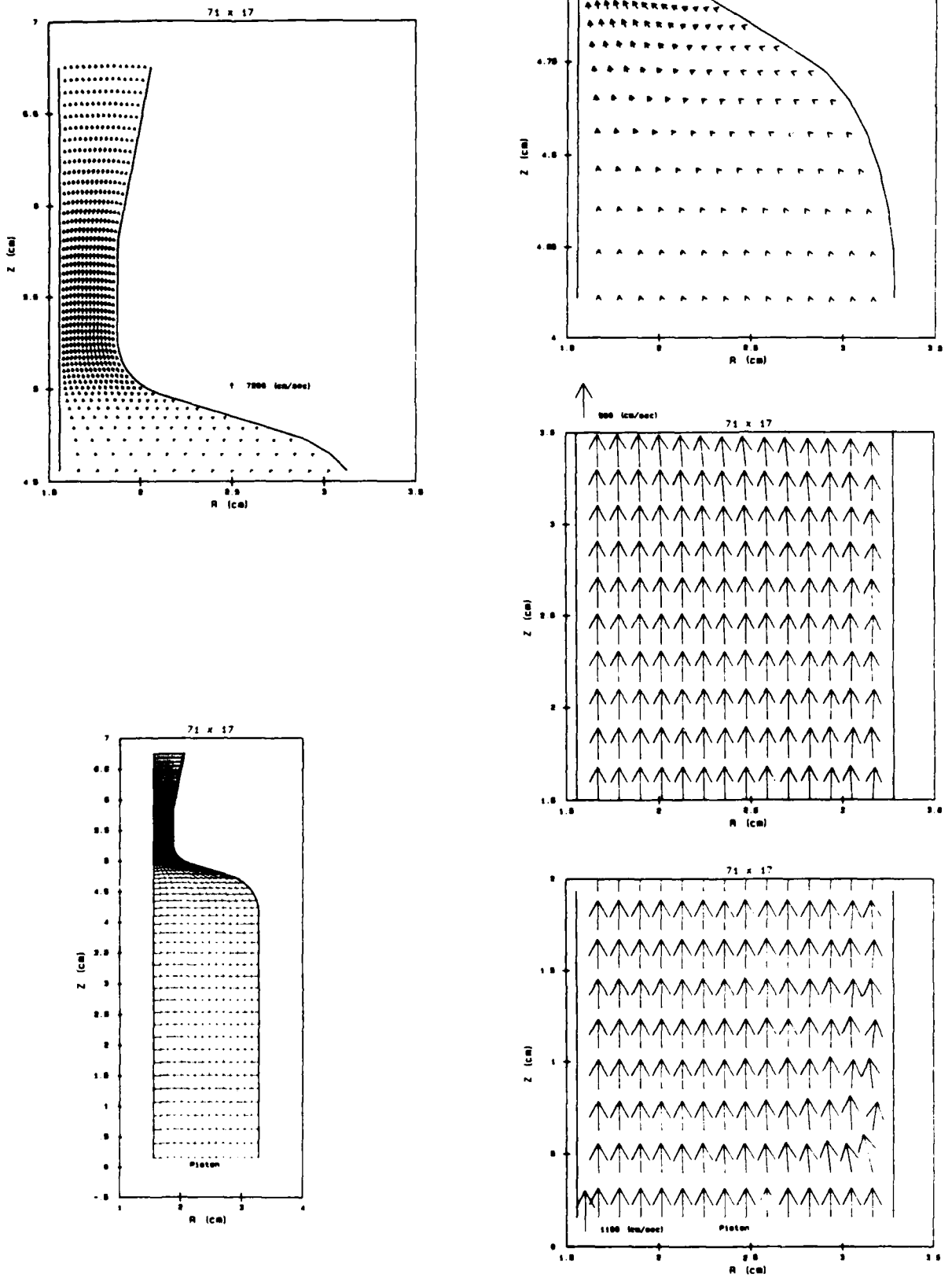

Fig. 3.11. Grid distribution and velocity-vector plots for Run No. 1 of GE; (a) t = 0.4 msec.

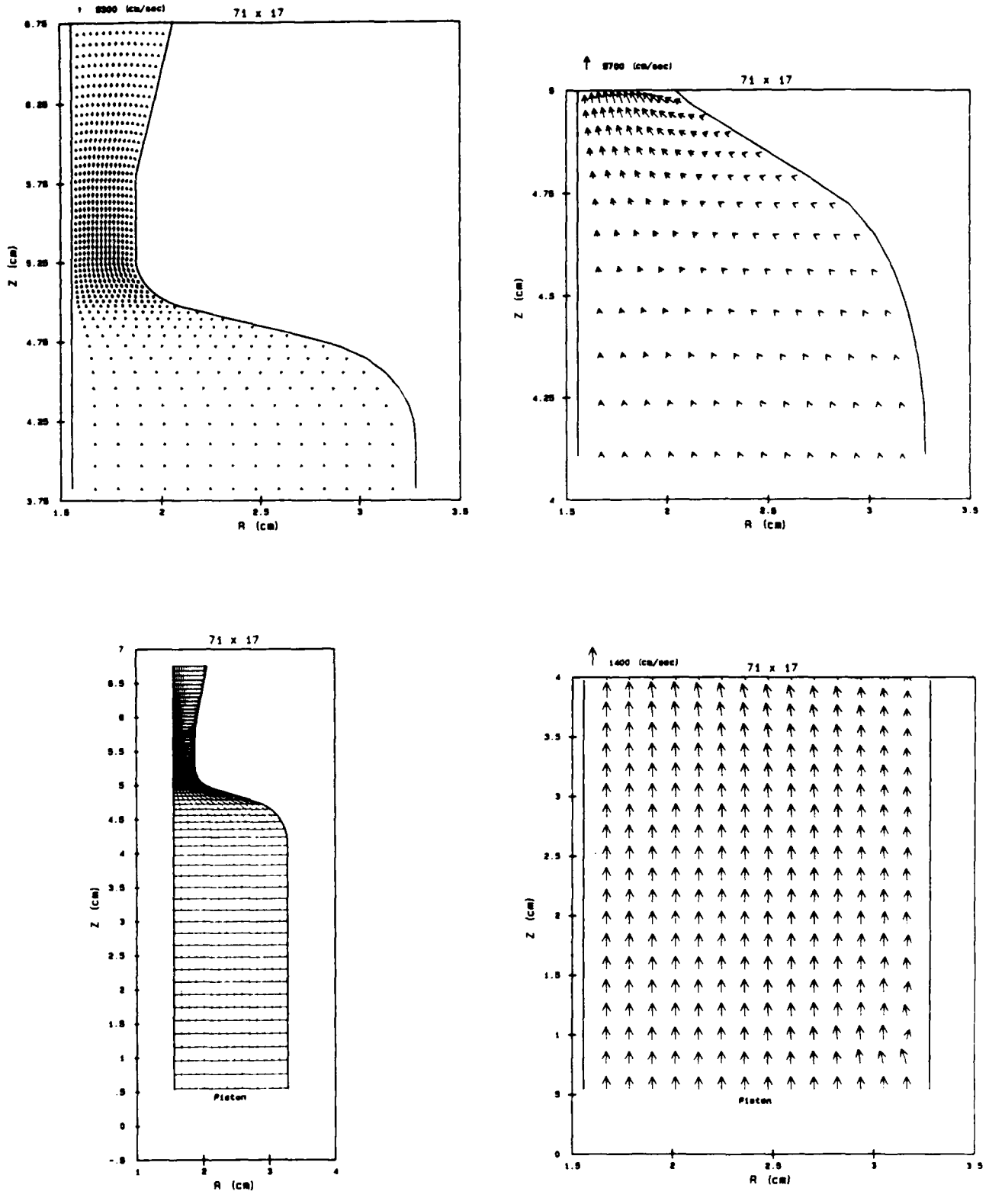

Fig. 3.11 (Continued). (b) t = 0.8 msec.

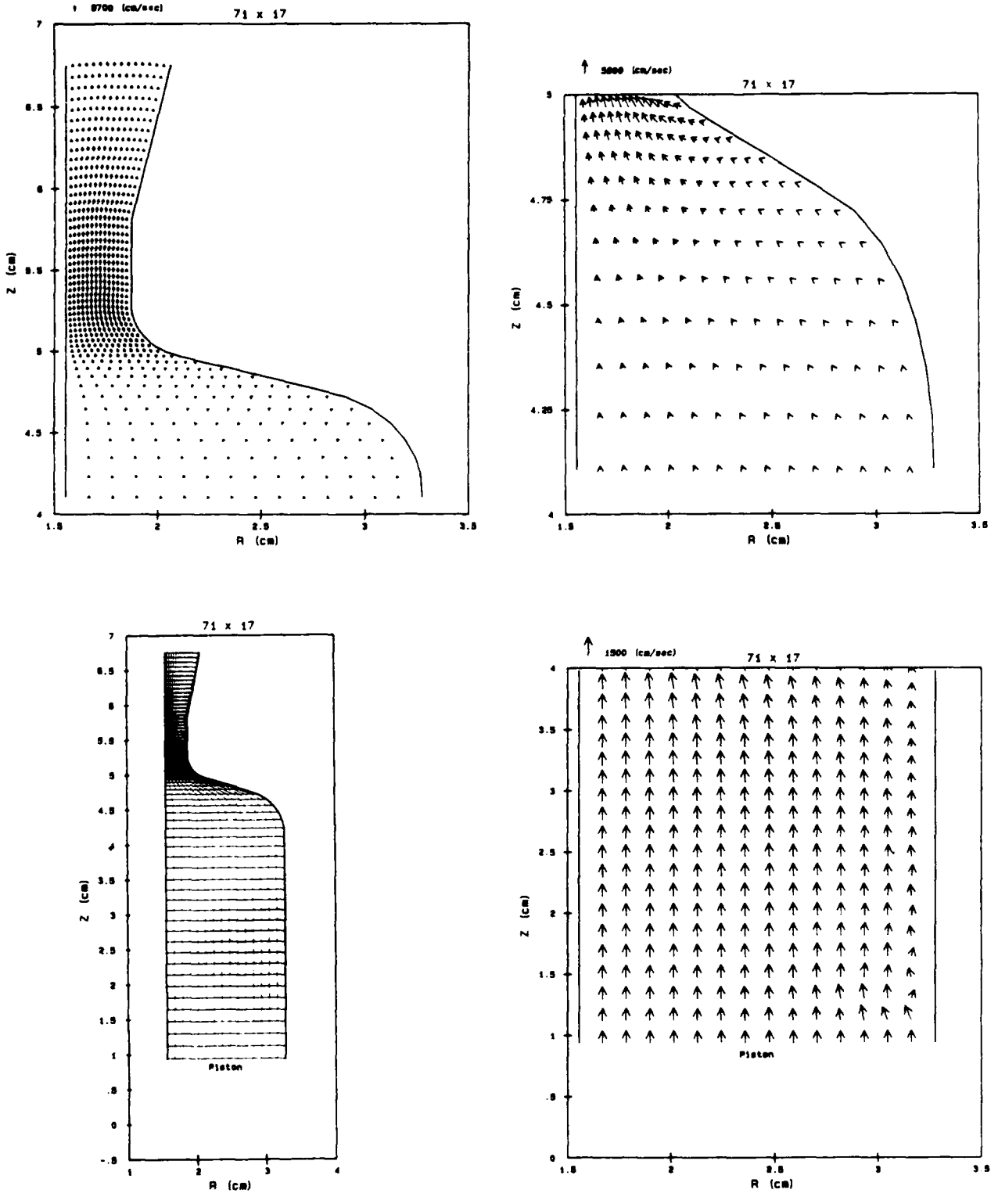

Fig. 3.11 (Continued). (c) t = 1.2 msec.

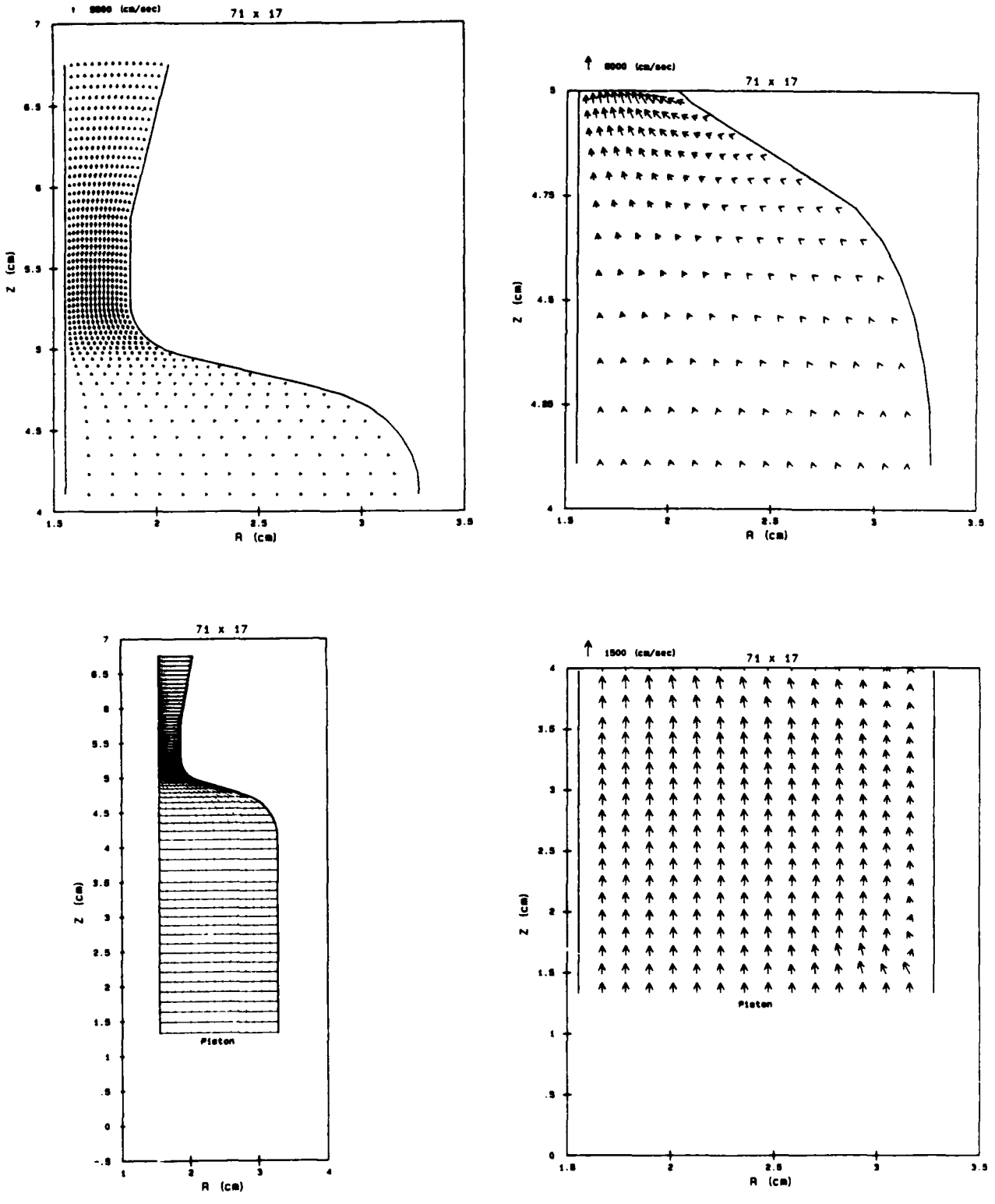

Fig. 3.11. (Continued). (d) t = 1.6 msec.

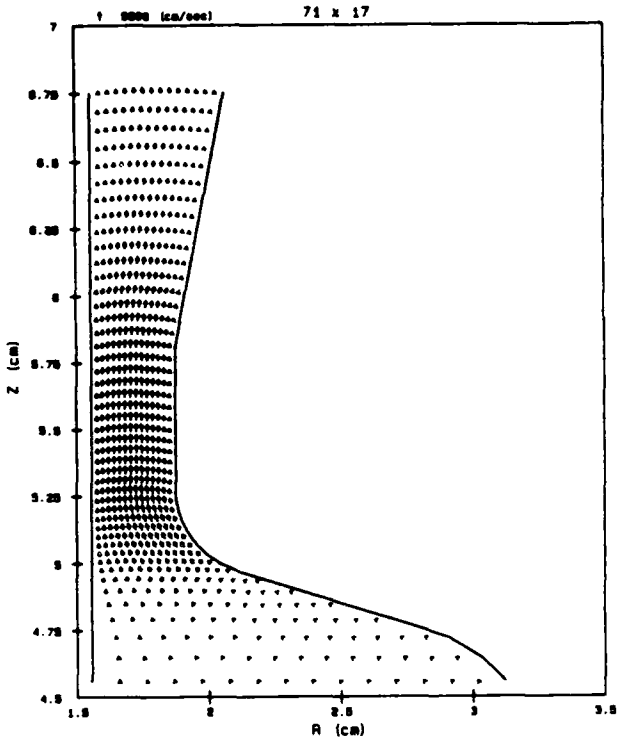

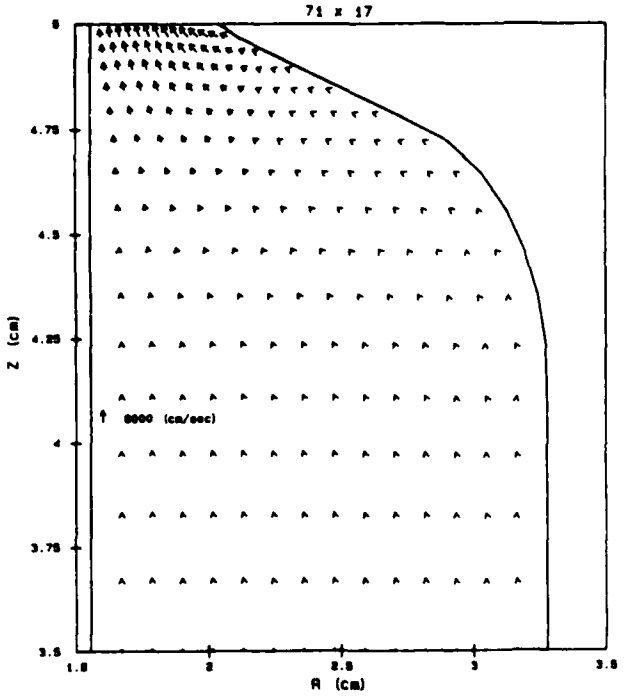

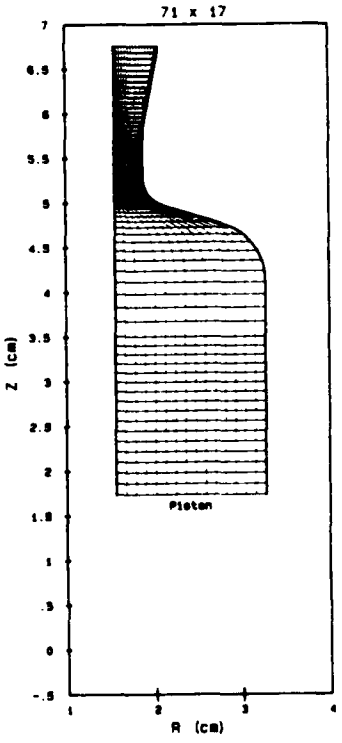

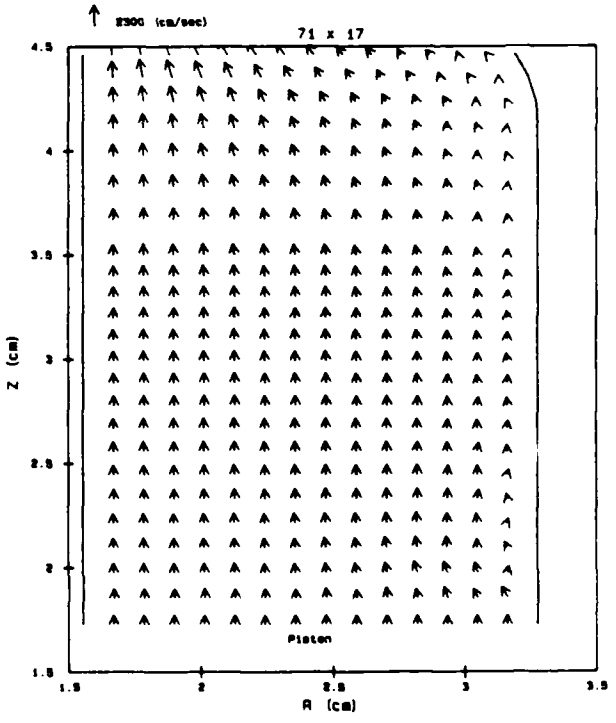

Fig. 3.11. (Continued). (e) t = 2.0 msec.

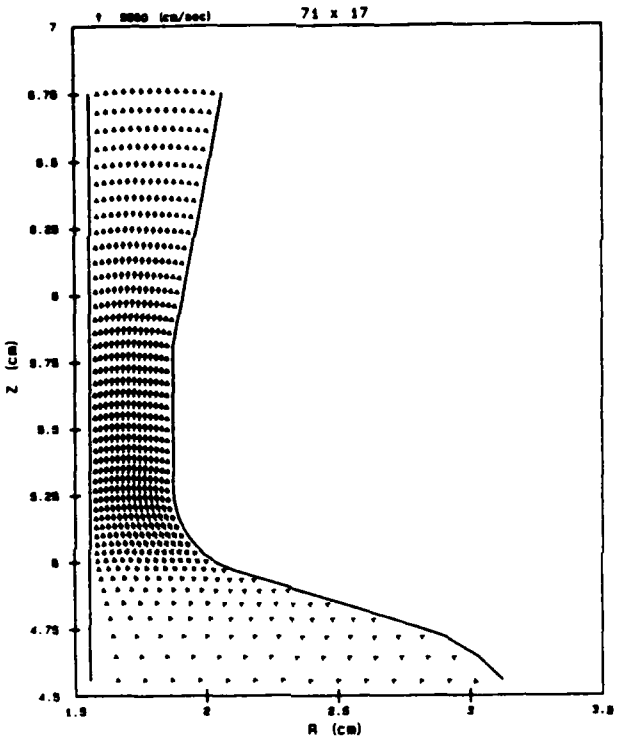

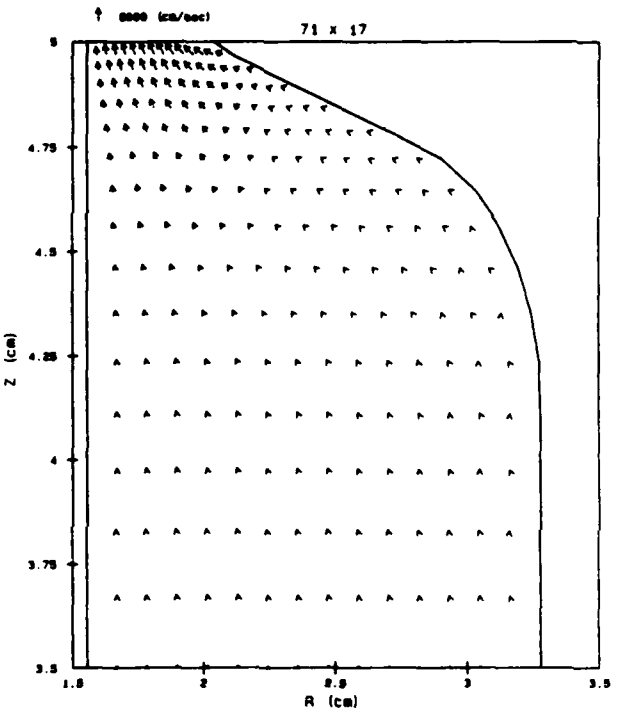

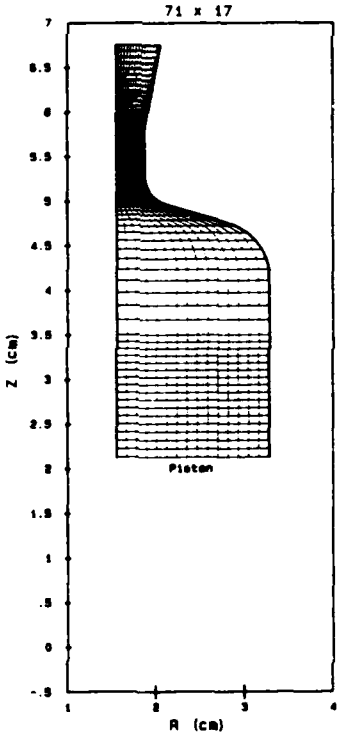

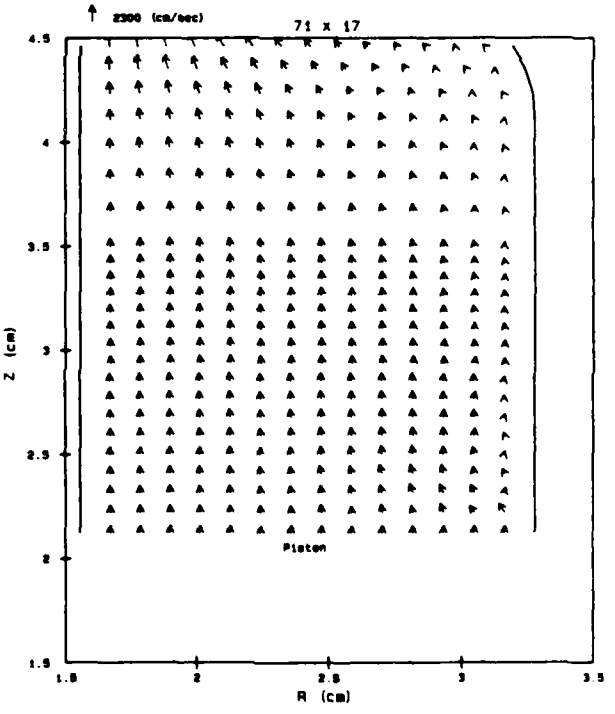

Fig. 3.11. (Continued). (f) t = 2.4 msec.

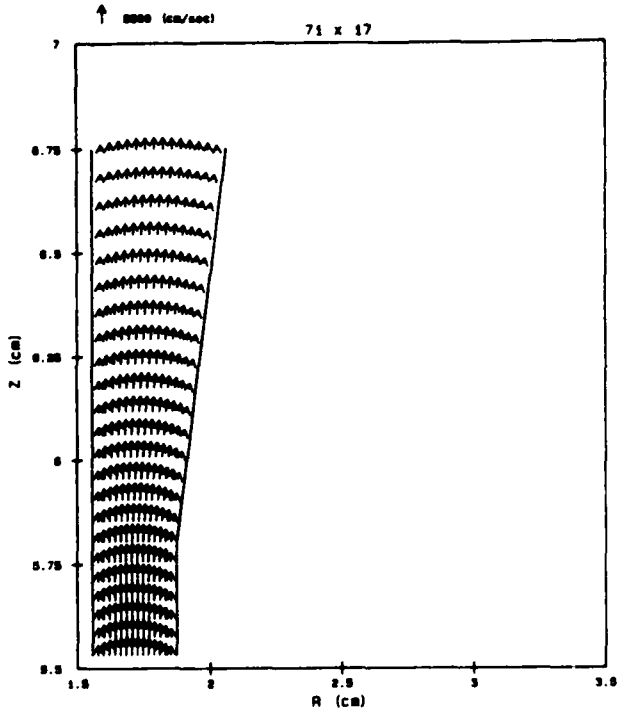

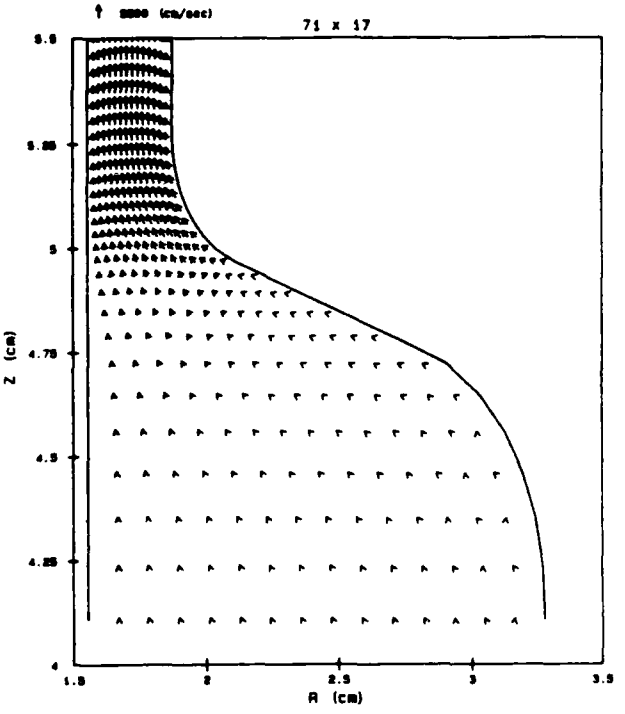

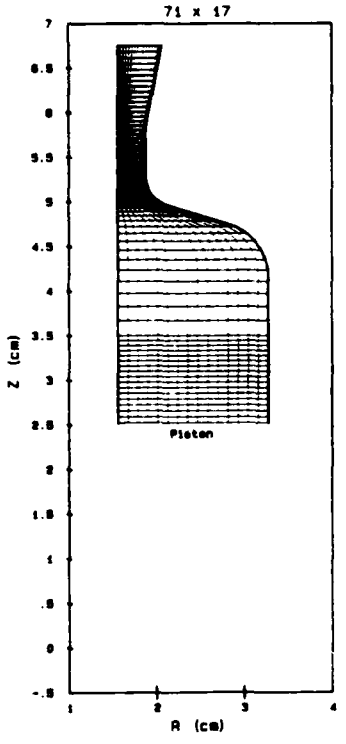

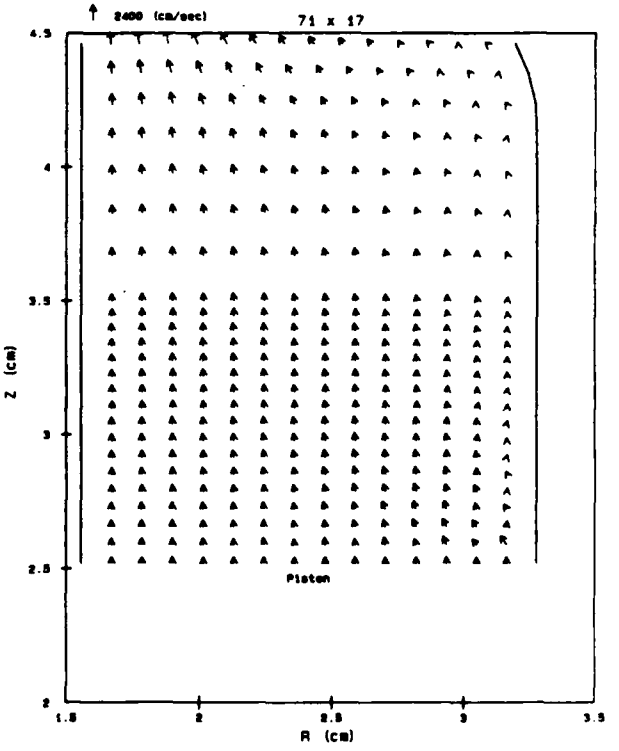

Fig. 3.11. (Continued). (g) t = 2.8 msec.

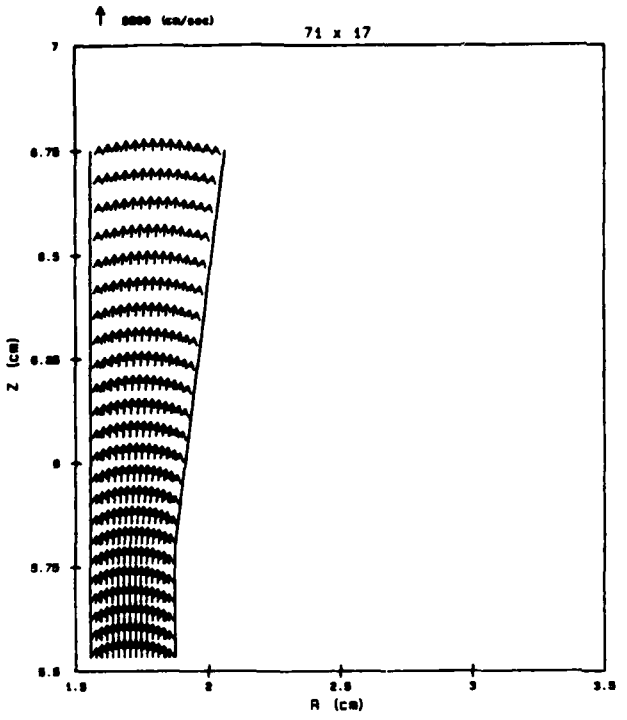

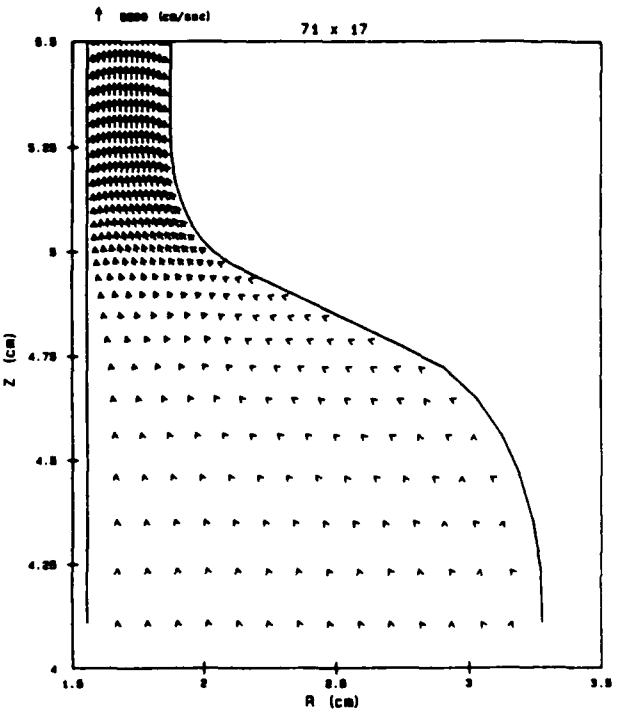

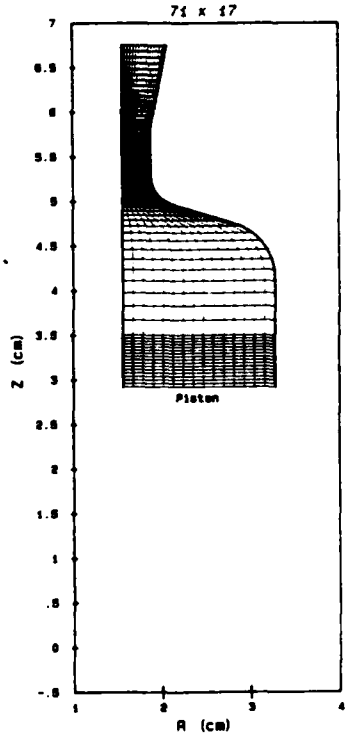

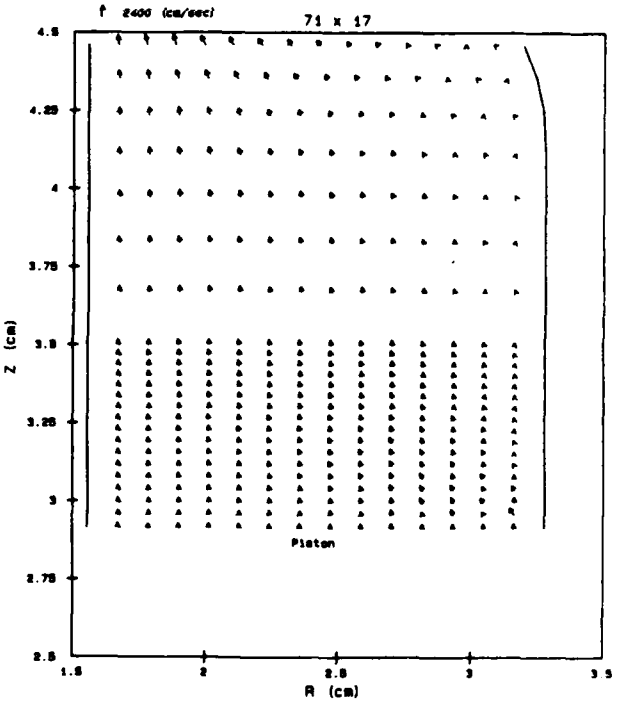

Fig. 3.11. (Continued). (h) t = 3.2 msec.

zone to go beyond the limits of 0.8-1.2. Attempts to carry out the calculations to significantly longer times have shown that the cells collapse, resulting in a very large aspect ratio for the moving-grid cells. This occurrence is another source of unstable behavior.

Figure 3.12 shows the plot of discharge coefficient as a function of time for Run No. 1 of GE, for which the velocity-vector plots were presented in Fig. 3.11. The discharge coefficient approaches a value of 0.76 at the longer times compared to the corrected, experimental steady-state value of 0.99. The effect of numerical diffusion is evident in this result.

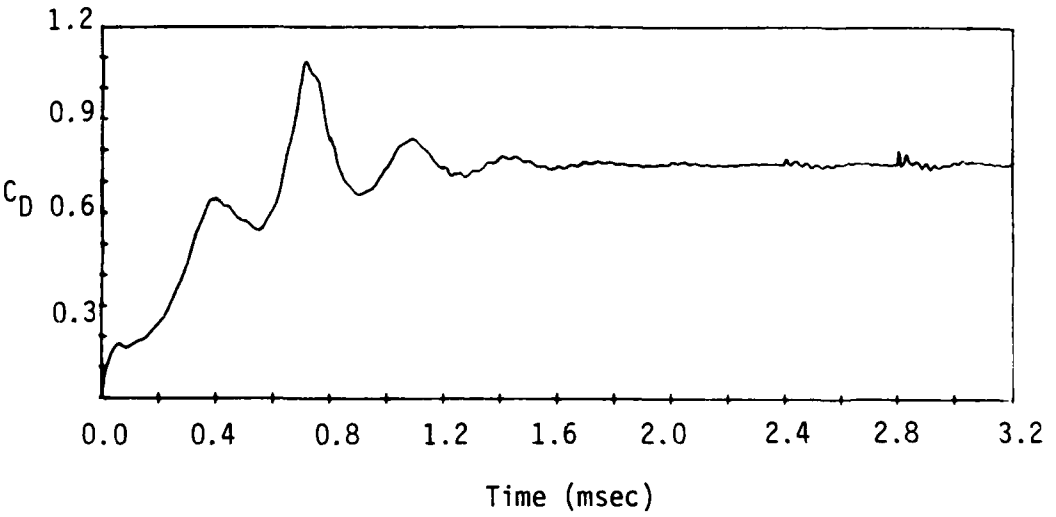

Fig. 3.12. Predicted discharge coefficient vs. time for Run No. 1 of GE.

4. DISCUSSION AND CONCLUSION

This research activity has involved the development of a 2-D transient simulation of the interior ballistics process in regenerative liquid-propellant guns. The focus of the research has been on the description of the flow inside the injector covering the domain of the flow path from the propellant chamber to the exit of the annular orifice injector.

There were three features of this LPG research: (1) The delineation of the phenomena occurring in the fluid prior to injection into the combustion chamber, whereas other research is focused largely on the post-injection process, (2) The inclusion of the highly transient nature of the injection/orifice flow process, whereas prior research on orifice flow is almost exclusively limited to steady flow, and (3) The 2-D description of the flow that is necessary to investigate the occurrance of vortex roll-up in the propellant chamber, to study the development of internal recirculation zones, and to delineate the relationship between the phenomena occurring inside the injector and the occurrence of pressure fluctuations observed in experimental gun firing.

This report presents the prediction of the onset and temporal growth of recirculation zones inside an orifice with fixed, spatially varying cross-sectional area, the direct prediction of discharge coefficients for time-varying, i.e., moving-boundary, orifice flows, and a study of grid resolution effects in a straight annular orifice for which an analytical solution for steady flow exists (Poisuille flow).

In addition to the physical phenomena predicted by the model, an important conclusion derived from these results was the existence of numerical diffusion in the calculations. Although the Poisuille-flow study showed that with a coarse grid the predicted solution deviated from the analytic solution, a modest refinement in the grid produced excellent agreement with the exact

solution. However, when the model was applied to a typical LPG orifice-flow geometry with the moving boundary, numerical diffusion was not reduced to an acceptable level. The basic method in the existing calculation involves a first-order upwind differencing of the convective terms. The advantage is stability, but the penalty is accuracy. Methods that take advantage of the existing low-order, but stable solution, to compute the correction terms that are used to compute an updated low-order solution should result in mitigating the accuracy problem, affecting an increase in accuracy of the basic differencing method.

Although the results show the onset of vortex generation in the propellant chamber due to the moving boundary, the requirement exists for increasing the resolution of the wall boundary layer as a means of accurately describing it to study the potential vortex roll-up phenomenon and the regions of steep gradients.

In addition, a re-gridding technique is needed which provides for maintaining good aspect ratios and adjacent-cell ratios throughout the entire injection process. While the new re-gridding helps to eliminate the aspect-ratio problem, it also provides the means for moving the upper wall and keeping the piston and the lower wall fixed, resulting in a geometery and piston movement similar to the experimental configurations, i.e., the piston moving opposite to the direction of injection.

Acknowledgements

This work was supported by the U.S. Army Research Office with Dr. David Mann as the project monitor. The authors would like to thank Drs. Robert Schlaug, Fred Su and C.C. Hsiao of SAIC, and Dr. Terence Coffee of the BRL for helpful discussions.

References

1. Phillips, G., Murty, S., Traci, R., and Edelman, R.B., "Analysis of Interior Ballistics Process of Bulk Loaded Liquid Propellant Guns," 17th JANNAF Combustion Meeting, CPIA Publication 329, Vol. III, pp. 403-448, 1980.

2. "A User's Guide for the MAGIC Fluids Simulation Model," Report SAIC-86/6554, Science Applications International Corporation, 10210 Campus Point Drive, San Diego, CA 92121, July 1987.

3. Pagan, G. and Izod, D.C.A., "Regenerative Liquid Propellant Gun Modeling," Proceedings of the Seventh International Symposium on Ballistics, The Hague, The Netherlands, April 1983.

4. Cushman, P.G., "Regenerative Liquid Propellant Gun Simulation User's Manual," GE Report 84-POD-004, December 1983.

5. Gough, P.S., "A Model of the Interior Ballistics of Hybrid Liquid-Propellant Guns," Final Report, PGA-TR-83-4, Paul Gough Associates, Inc. Portsmouth, NH 03801, September 1983.

6. Coffee, T.P., "A Lumped Parameter Code for Regenerative Liquid Propellant Guns," BRL-TR-2703, December 1985.

7. Coffee, T.P., "The Analysis of Experimental Measurements for Liquid Regenerative Guns," Technical Report BRL-TR-2731, May 1986.

8. Coffee, T.P., "One-Dimensional Modeling of Liquid Injection in a Regenerative Propellant Gun," Technical Report BRL-TR-2897, March 1988.

9. Morrison, W.F. and Wren, G.P., "A Model of Liquid Injection in a Regenerative Liquid Propellant Gun," Technical Report BRL-TR-2851, July 1987.

10. Pate, R.A., private communication, General Electric, Ordnance Systems Division, Pittsfied, MA, 1985.

11. Morrison, C. and Edelman, A., "An Experimental Device for the Study of Transient Flow of Liquids in LPG Injectors," 24th JANNAF Combustion Meeting, Monterey, California, October 5-9, 1987.